REMARKS

Claims 1-28 and 45-85 remain in this application. Claims 9, 26, 29-44, 49, 66, 77, and 85-89 have been withdrawn.

I. CLAIM REJECTIONS – 35 U.S.C. § 112

A. Examiner's Statements

The Examiner rejected claims 2, 16, 45, and 56 under 35 U.S.C. § 112, second paragraph, as being indefinite for failing to particularly point out and distinctly claim the subject matter which applicant regards as the invention.

The Examiner stated that the terms "mini'", "micro" in claims 16 and 56 are relative terms, which render the claims indefinite. The Examiner stated that terms mini-", "micro" are not defined by the claims, the specification does not provide a standard for ascertaining the requisite degree, and one of ordinary skill in the art would not be reasonably apprised of the scope of the invention. The Examiner stated, therefore, the Examiner considers any pump for pumping milli-units as a mini-pump.

The Examiner stated that the term "micro-capillary" in claims 2 and 45 is a relative term which renders the claims indefinite. The Examiner stated that the term "micro-capillary" is not defined by the claim, the specification does not provide a standard for ascertaining the requisite degree, and one of ordinary skill in the art would not be reasonably apprised of the scope of the scope of the invention. The Examiner stated, therefore, that the Examiner considers that the heat exchanged used with an electronic thermal component is a micro-capillary exchanger for its small size.

B. Law

A claim may not be rejected solely because of the type of language used to define the subject matter for which patent protection is sought.[1] In reviewing a claim for compliance with 35 U.S.C. 112, second paragraph, the examiner must consider the claim as a whole to determine whether the claim apprises one of ordinary skill in the art of its scope and, therefore, serves the notice function required by 35 U.S.C. 112, second paragraph, by providing clear warning to others as to what constitutes infringement of the patent.[2] Breadth of a claim is not to be equated with

---

[1] *In re Swinehart*, 439 F.2d 210, 160 USPQ 226 (CCPA 1971).

[2] *See, e.g., Solomon v. Kimberly-Clark Corp.*, 216 F.3d 1372, 1379, 55 USPQ2d 1279, 1283 (Fed. Cir. 2000).

indefiniteness.[3] If the claims, read in light of the specification, reasonably apprise those skilled in the art both of the utilization and scope of the invention, and if the language is as precise as the subject matter permits, the statute [35 U.S.C. §112, second paragraph] demands no more.[4]

C.   Claims 16 and 56

Claims 16 and 56 require a pump selected from the group consisting of a mini-pump or a micro-pump. Although, the Examiner stated that one of ordinary skill in the art would not be reasonably appraised of the scope of the invention, the terms "mini" and "micro" used in reference to pumps are in fact terms of art. Applicants attach as Appendix A, published articles and Internet product brochures showing industry use of the terms "mini" and "micro" in reference to pumps. Applicants respectfully submit that one of ordinary skill in the art would be reasonably appraised of the scope of the invention of claims 16 and 56 because "mini" and "micro" are standard industry terms with respect to pumps. Applicants therefore respectfully request that the Examiner withdraw the rejection of claims 16 and 56.

D.   Claims 2 and 45

Claims 2 and 45 require a "micro-capillary, cold plate heat exchanger". Although, the Examiner stated that one of ordinary skill in the art would not be reasonably appraised of the scope of the invention, the term "micro-capillary" used in reference to a heat exchanger is in fact a term of art. Applicants attach as Appendix B, a published article showing industry use of the term "micro-capillary" in reference to heat exchangers as being interchangeable with the term "micro-channel" in reference to heat exchangers. Applicants direct the Examiner's attention to endnote [9] and the reference made thereto in the article. Applicants respectfully submit that one of ordinary skill in the art would be reasonably appraised of the scope of the invention of claims 2 and 45 because "micro-capillary" is a standard industry term with respect to heat exchangers. Applicants therefore respectfully request that the Examiner withdraw the rejection of claims 2 and 45.

---

[3] *In re Miller*, 441 F.2d 689, 169 USPQ 597 (CCPA 1971).

[4] *Shatterproof Glass Corp. v. Libbey Owens Ford Co.*, 758 F.2d 613, 225 USPQ 634 (Fed. Cir. 1985); *Hybritech, Inc. v. Monoclonal Antibodies, Inc.*, 802 F.2d 1367, 231 USPQ 81 (Fed. Cir. 1986).

141514.01/1391.34500

II. CLAIM REJECTIONS – 35 U.S.C. § 102

A. Examiner's Statements

The Examiner rejected claims 1, 3, 7-8, 10-11, 25, 27-28 under 35 U.S.C. § 102(b) as being anticipated by Chrysler et al. (U.S. Patent No. 5,456,081) [hereinafter Chrysler]. The Examiner rejected claims 1, 4-5, 10-14, 25, 27-28 under 35 U.S.C. § 102(e) as being anticipated by Chou et al. (U.S. Patent Application Publication No. 20020144811) [hereinafter Chou]. The Examiner rejected claims 1, 2, 4-5, 45, 47, 48, 50-51, 65, 67-73, 75-76, 78-81, 83-84 under 35 U.S.C.§ 102(e) as being anticipated by Parish et al. (U.S. Patent Application Publication No. 20030136548) [hereinafter Parish].

B. Law

A claim is anticipated only if each and every element as set forth in the claim is found, either expressly or inherently described, in a single prior art reference.[5] The identical invention must be shown in as complete detail as is contained in the ... claim.[6] To establish inherency, the extrinsic evidence "must make clear that the missing descriptive matter is necessarily present in the thing described in the reference, and that it would be so recognized by persons of ordinary skill. Inherency, however, may not be established by probabilities or possibilities. The mere fact that a certain thing may result from a given set of circumstances is not sufficient."[7] Thus, the fact that a certain result or characteristic <u>may</u> occur or be present in the prior art is not sufficient to establish inherency of that result or characteristic.[8] In relying upon the theory of inherency, the examiner must provide a basis in fact and/or technical reasoning to reasonably support the determination that the allegedly inherent characteristic <u>necessarily</u> flows from the teachings of the applied prior art.[9] In addition to disclosing every claim limitation, an anticipatory prior art reference must enable the practice of the invention and describe it sufficiently to have placed it in the possession of a person of ordinary skill in the field of the invention.[10]

---

[5] *Verdegaal Bros. v. Union Oil Co. of California*, 814 F.2d 628, 631, 2 USPQ2d 1051, 1053 (Fed. Cir. 1987).

[6] *Richardson v. Suzuki Motor Co.*, 868 F.2d 1226, 1236, 9 USPQ2d 1913, 1920 (Fed. Cir. 1989).

[7] *In re Robertson*, 169 F.3d 743, 745, 49 USPQ2d 1949, 1950-51 (Fed. Cir. 1999).

[8] *In re Rijckaert*, 9 F.3d 1531, 1534, 28 USPQ2d 1955, 1957 (Fed. Cir. 1993).

[9] *Ex parte Levy*, 17 USPQ2d 1461, 1464 (Bd. Pat. App. & Inter. 1990).

[10] *In re Paulsen*, 30 F.3d 1475, 1478-79 (Fed. Cir. 1994).

C. Chrysler Does Not Anticipate Claims 1, 3, 7-8, 10-11, 25, and 27-28

Applicants have amended independent claim 1 to overcome the Office's rejections. Claims 3, 7-8, 10-11, 25, and 27-28 either directly or indirectly depend from claim 1. Chrysler does not teach or disclose at least a heat exchanger, a heat storage unit, and a thermal conduit system in a downhole tool. Therefore, applicants respectfully submit that Chrysler does not anticipate claims 1, 3, 7-8, 10-11, 25, and 27-28 because Chrysler does not disclose each of the claim limitations. Applicants therefore respectfully request that the Examiner withdraw the rejection of claims 1, 3, 7-8, 10-11, 25, and 27-28.

D. Chou Does Not Anticipate Claims 1, 4-5, 10-14, 25, and 27-28

Applicants have amended independent claim 1 to overcome the Office's rejections. Claims 4-5, 10-14, 25, and 27-28 depend either directly or indirectly from claim 1. Chou does not anticipate claims 1, 4-5, 10-14, 25, and 27-28 because Chou does not disclose a heat exchanger, heat storage unit, and thermal conduit system being in a downhole tool, as required by the claims. Therefore, applicants respectfully submit that Chou does not anticipate claims 1, 4-5, 10-14, 25, and 27-28 because Chou does not disclose each of the claim limitations. Applicants therefore respectfully request that the Examiner withdraw the rejection of claims 1, 4-5, 10-14, 25, and 27-28.

E. Parish Does Not Anticipate Claims 1, 2, 4-5, 45, 47, 48, 50-51, 65, 67-73, 75-76, 78-81, and 83-84

Applicants have amended independent claims 1, 45, 69, and 78 to overcome the Office's rejections. Claims, 2, and 4-5 depend either directly or indirectly from claim 1. Claims 47, 48, 50-51, 65, 67-68 depend either directly or indirectly from claim 45. Claims 70-73 and 75-76 depend either directly or indirectly from claim 69. Claims 79-81 and 83-84 depend either directly or indirectly from claim 78. Parish does not anticipate claims 1, 2, 4-5, 45, 47, 48, 50-51, 65, 67-73, 75-76, 78-81, and 83-84 because Parish does not disclose a heat exchanger, heat storage unit, and thermal conduit system being in a downhole tool, as required by the claims. Therefore, applicants respectfully submit that Parish does not anticipate claims 1, 2, 4-5, 45, 47, 48, 50-51, 65, 67-73, 75-76, 78-81, and 83-84 because Parish does not disclose each of the claim limitations. Applicants therefore respectfully request that the Examiner withdraw the rejection of claims 1, 2, 4 5, 45, 47, 48, 50-51, 65, 67-73, 75-76, 78-81, and 83-84.

III.   CLAIMS REJECTIONS – 35 U.S.C. § 103

A.   Examiner's Statements

The Examiner rejected claims 1, 10, and 11 under 35 U.S.C. §103 (a) as being unpatentable over Chen et al. (U.S. Patent No. 5,713,208) [hereinafter Chen] in view of Chrysler. The Examiner rejected claims 1, 3-5, 10-11, 15-16, and 25 under 35 U.S.C. § 103(a) as being unpatentable over Simmons et al. (U.S. Patent No. 6,481,216) [hereinafter Simmons] in view of Chrysler. The Examiner rejected claim 6 under 35 U.S.C. § 103(a) as being unpatentable over Chrysler in view of Bennett (U.S. Patent No. 5,165,243) [hereinafter Bennett]. The Examiner rejected claims 6, 46, 74, and 82 under 35 U.S.C. § 103(a) as being unpatentable over Parish in view of Bennett. The Examiner rejected claims 52-54 under 35 U.S.C. § 103(a) as being unpatentable over Parish in view of Chou. The Examiner rejected claims 55-56 under 35 U.S.C. § 103(a) as being unpatentable over Parish in view of Simmons. The Examiner rejected claims 17, 19, 21, and 23 under 35 U.S.C. § 103(a) as being unpatentable over Chrysler in view of Marsala (U.S. Patent No. 6,519,955) [hereinafter Marsala]. The Examiner rejected claims 57, 59, 61, and 63 under 35 U.S.C. § 103(a) as being unpatentable over Parish in view of Marsala. The Examiner rejected claims 18, 20, 22, and 24 under 35 U.S.C. § 103(a) as being unpatentable over Chrysler and Marsala as applied to claims 17, 19, 21, and 23 above, and further in view of Simmons. The Examiner rejected claims 58, 60, 62, and 64 under 35 U.S.C. § 103(a) as being unpatentable over Parish and Marsala as applied to claims 57, 59, 61, and 63 above, and further in view of Simmons.

B.   Law

The examiner bears the initial burden of factually supporting any *prima facie* conclusion of obviousness. To establish a *prima facie* case of obviousness, three basic criteria must be met. First, there must be some suggestion or motivation, either in the references themselves or in the knowledge generally available to one of ordinary skill in the art, to modify the reference or to combine reference teachings.[11] Second, there must be a reasonable expectation of success.[12] Finally, the prior art reference, or references when combined, must teach or suggest all the claim limitations.[13] The teaching or suggestion to make the claimed combination and the reasonable

---

[11] *In re Vaeck*, 947 F.2d 488, 20 USPQ2d 1438 (Fed. Cir. 1991).

[12] *In re Vaeck*, 947 F.2d 488, 20 USPQ2d 1438 (Fed. Cir. 1991).

[13] *In re Vaeck*, 947 F.2d 488, 20 USPQ2d 1438 (Fed. Cir. 1991).

141514.01/1391.34500

expectation of success must both be found in the prior art, and not based on applicant's disclosure.[14]

There are three possible sources for a motivation to combine references: (1) the nature of the problem to be solved; (2) the teachings of the prior art; and (3) the knowledge of persons of ordinary skill in the art.[15] The mere fact that references can be combined or modified does not render the resultant combination obvious unless the prior art also suggests the desirability of the combination.[16] Thus, a statement that modifications of the prior art to meet the claimed invention would have been "'well within the ordinary skill of the art at the time the claimed invention was made'" because the references relied upon teach that all aspects of the claimed invention were individually known in the art is not sufficient to establish a *prima facie* case of obviousness without some objective reason to combine the teachings of the references.[17]

Also, if the proposed modification would render the prior art invention being modified unsatisfactory for its intended purpose, then there is no suggestion or motivation to make the proposed modification.[18] In addition, if the proposed modification or combination of the prior art would change the principle of operation of the prior art invention being modified, then the teachings of the references are not sufficient to render the claims *prima facie* obvious.[19]

C. Claims 1, 10, And 11 Are Not Unpatentable Over Chen In View Of Chrysler

Applicants have amended claim 1 to include the limitation of a heat exchanger, heat storage unit, and thermal conduit system being in a downhole tool. Claims 1, 10, and 11 are not unpatentable over Chen in view of Chrysler because Chen as combined with Chrysler does not teach or suggest a heat exchanger, heat storage unit, and thermal conduit system being in a downhole tool, as required by the claims. Applicants respectfully submit that Chen as combined with Chrysler does not render claims 1, 10, and 11 obvious because Chen as combined with

---

[14] *In re Vaeck*, 947 F.2d 488, 20 USPQ2d 1438 (Fed. Cir. 1991).

[15] *In re Rouffet*, 149 F.3d 1350, 1357, 47 USPQ2d 1453, 1457-58 (Fed. Cir. 1998).

[16] *In re Mills*, 916 F.2d 680, 16 USPQ2d 1430 (Fed. Cir. 1990); *see also In re Fritch*, 972 F.2d 1260, 23 USPQ2d 1780 (Fed. Cir. 1992).

[17] *Ex parte Levengood*, 28 USPQ2d 1300 (Bd. Pat. App. & Inter. 1993); *see also In re Kotzab*, 217 F.3d 1365, 1371, 55 USPQ2d 1313, 1318 (Fed. Cir. 2000); *Al-Site Corp. v. VSI Int'l Inc.*, 174 F.3d 1308, 50 USPQ2d 1161 (Fed. Cir. 1999).

[18] *In re Gordon*, 733 F.2d 900, 221 USPQ 1125 (Fed. Cir. 1984).

[19] *In re Ratti*, 270 F.2d 810, 123 USPQ 349 (CCPA 1959).

Chrysler does not teach or suggest all of the claim limitations. Applicants therefore respectfully request that the Examiner withdraw the rejection of claims 1, 10, and 11.

D.   Claims 1, 3-5, 10-11, 15-16, And 25 Are Not Unpatentable Over Simmons In View Of Chrysler

Applicants have amended claim 1 to include the limitation of heat exchanger, heat storage unit, and thermal conduit system being in a downhole tool. Claims 1, 3-5, 10-11, 15-16, and 25 are not unpatentable over Simmons in view of Chrysler because Simmons as combined with Chrysler does not teach or suggest a heat exchanger, heat storage unit, and thermal conduit system being in a downhole tool, as required by the claims. Applicants respectfully submit that Simmons as combined with Chrysler does not render claims 1, 3-5, 10-11, 15-16, and 25 obvious because Simmons as combined with Chrysler does not teach or suggest all of the claim limitations. Applicants therefore respectfully request that the Examiner withdraw the rejection of claims 1, 3-5, 10-11, 15-16, and 25.

E.   Claim 6 Is Not Unpatentable Over Chrysler In View of Bennett

Applicants have amended claim 1 to include the limitation of heat exchanger, heat storage unit, and thermal conduit system being in a downhole tool. Claim 6 depends from claim 1, therefore, claim 6 is not unpatentable over Chrysler in view of Bennett because Chrysler as combined with Bennett does not teach or suggest the limitation of a heat exchanger, heat storage unit, and thermal conduit system being in a downhole tool. Applicants respectfully submit that Chrysler as combined with Bennett does not render claim 6 obvious because Chrysler as combined with Bennett does not teach or suggest all of the claim limitations. Applicants therefore respectfully request that the Examiner withdraw the rejection of claim 6.

F.   Claims 6, 46, 74, And 82 Are Not Unpatentable Over Parish In View Of Bennett

Applicants have amended claims 1, 45, 69, and 78 to include the limitation of heat exchanger, heat storage unit, and thermal conduit system being in a downhole tool. Claim 6 depends from claim 1. Claim 46 depends from claim 45. Claim 74 depends from claim 69. Claim 82 depends from claim 78. Claims 6, 46, 74, and 82 are not unpatentable over Parish in view of Bennett because Parish as combined with Bennett does not teach or suggest the limitation of a heat exchanger, heat storage unit, and thermal conduit system being in a downhole tool. Applicants respectfully submit that Parish as combined with Bennett does not render claims 6, 46,

74, and 82 obvious because Parish as combined with Bennett does not teach or suggest all of the claim limitations. Applicants therefore respectfully request that the Examiner withdraw the rejection of claims 6, 46, 74, and 82.

G. Claims 52-54 Are Not Unpatentable Over Parish In View Of Chou

Applicants also repeat the arguments made above for the patentability of claim 45. As claims 52-54 depend from claim 45, Applicants respectfully submit that claims 52-54 are also patentable. Applicants therefore respectfully request that the Examiner withdraw the rejection of claims 52-54.

H. Claims 55-56 Are Not Unpatentable Over Parish In View Of Simmons

Applicants also repeat the arguments made above for the patentability of claim 45. As claims 55-56 depend from claim 45, Applicants respectfully submit that claims 55-56 are also patentable. Applicants therefore respectfully request that the Examiner withdraw the rejection of claims 55-56.

I. Claims 17, 19, 21, And 23 Are Not Unpatentable Over Chrysler In View Of Marsala

Applicants repeat the arguments made above for the patentability of claim 1. As claims 17, 19, 21, and 23 depend from claim 1, applicants respectfully submit that claims 17, 19, 21, and 23 are also patentable. Applicants therefore respectfully request that the Examiner withdraw the rejection of claims 17, 19, 21, and 23.

J. Claims 57, 59, 61, And 63 Are Not Unpatentable Over Parish In View Of Marsala

Applicants repeat the arguments made above for the patentability of claim 45. As claims 57, 59, 61, and 63 depend from claim 45, applicants respectfully submit that claims 57, 59, 61, and 63 are also patentable. Applicants therefore respectfully request that the Examiner withdraw the rejection of claims 57, 59, 61, and 63.

K. Claims 18, 20, 22, And 24 Are Not Unpatentable Over Chrysler And Marsala And Further In View Of Simmons

Applicants repeat the arguments made above for the patentability of claim 1. As claims 18, 20, 22, and 24 depend from claim 1, applicants respectfully submit that claims 18, 20, 22, and 24 are also patentable. Applicants therefore respectfully request that the Examiner withdraw the rejection of claims 18, 20, 22, and 24.

141514.01/1391.34500

L. **Claims 58, 60, 62, And 64 Are Not Unpatentable Over Parish And Marsala And Further In View Of Simmons**

Applicants repeat the arguments made above for the patentability of claim 45. As claims 58, 60, 62, and 64 depend from claim 45, applicants respectfully submit that claims 58, 60, 62, and 64 are also patentable. Applicants therefore respectfully request that the Examiner withdraw the rejection of claims 58, 60, 62, and 64.

IV. AMENDMENTS MADE NOT RELATED TO PATENTABILITY

Applicants have amended claims 1, 10, 45, 50, 69-71, and 78-79 to more clearly, correctly, and properly claim the invention and not for purposes of patentability. Applicants have amended the term "heat sink" to "heat storage unit" to more accurately reflect the nature of the heat storage unit as described in the specification in light of the terminology used in some of the cited references.

These statements are not an admission that the other amendments were made for purposes of patentability, meant to be limiting in any way, or meant to be all-inclusive of amendments not made for purposes of patentability.

CONCLUSION

Applicants respectfully request reconsideration the pending claims and that a timely Notice of Allowance be issued in this case. If the Examiner feels that a telephone conference would expedite the resolution of this case, he is respectfully requested to contact the undersigned.
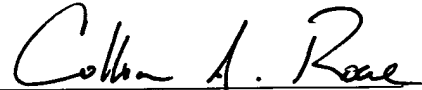
In the course of the foregoing discussions, Applicants may have at times referred to claim limitations in shorthand fashion, or may have focused on a particular claim element. This discussion should not be interpreted to mean that the other limitations can be ignored or dismissed. The claims must be viewed as a whole, and each limitation of the claims must be considered when determining the patentability of the claims. There may also be other distinctions between the claims and the prior art that have yet to be raised, but that may be raised in the future.

141514.01/1391.34500

If any fees are inadvertently omitted or if any additional fees are required or have been overpaid, please appropriately charge or credit those fees to Conley Rose, P.C. Deposit Account Number 03-2769 (ref. 1391-34500) of Conley Rose, P.C., Houston, Texas.

Respectfully submitted,

CONLEY ROSE, P.C.

Collin A. Rose
Reg. No. 47,036
P.O. Box 3267
Houston, TX 77253-3267
(713) 238-8000 (Phone)
(713) 238-8008 (Fax)

Attachments

141514.01/1391.34500

Appendix A

15 products ▪ micro pumps

4 products in ▪ dispensing : equipment and accessories
4 products in ▪ other pumps…
4 products in ▪ diaphragm pumps, peristaltic pumps
1 products in ▪ piston pumps, screw pumps, centrifugal pumps
1 products in ▪ vacuum pumps
▪ + Other …

4 products in ▪ dispensing : equipment and accessories

☐	**micro** dispensing stations ▪-info--	(mta)	mta automation ag
☐	**micro** dispensing systems	SCHMIDT	SCHMIDT Technology
☐	**micro** dispensing systems ▪-info--	microdrop	microdrop
☐	laboratory plate **micro** dispensing units	BRANDEL	Brandel

… see all the products in the category ▪ dispensing : equipment and accessories

4 products in ▪ other pumps…

☐	**micro-pumps** ▪-info ·	BIERI Hydraulik	Bieri Hydraulik
☐	custom made **micro** & mini **pumps** ▪-info	Namiki	Namiki
☐	custom made **micro** & mini **pumps**	☐ Diener Precision Pumps	Diener Precision Pumps
☐	mini bellow **pumps** ▪-info	GRI INDUSTRIES	Gorman-Rupp Industries ▪-PDF
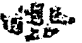
… see all the products in the category ▪ other pumps…

4 products in ▪ diaphragm pumps, peristaltic pumps

☐	**micro** & miniature diaphragm adjustable flow rate liquid **pumps** ▪-info	Namiki	Namiki

☐ micro & miniature diaphragm liquid **pumps** ▪-info··   *Namiki*   Namiki

☐ **micro** & miniature diaphragm **pumps** ▪-info·   *Namiki*   Namiki

☐ **micro** diaphragm **pumps** for gas sampling   ══KNF___   KNF NEUBERGER

... see all the products in the category ▪ diaphragm pumps, peristaltic pumps

1 products in ▪ piston pumps, screw pumps, centrifugal pumps

☐ mini-piston **pumps**   ☰ *Diener Precision Pumps*   Diener Precision Pumps

... see all the products in the category ▪ piston pumps, screw pumps, centrifugal pumps

1 products in ▪ vacuum pumps

☐ **micro** & miniature diaphragm compressors & vacuum **pumps** ▪-info·   *Namiki*   Namiki

... see all the products in the category ▪ vacuum pumps

1 products in ▪ electric generator sets

☐ **micro** hydro power generation sets   Kubota   KUBOTA Pumps

... see all the products in the category ▪ electric generator sets

⌐→   ⊂Documentation⊃   ⊂Quotation⊃

Press releases

New Micro Diaphragm pumps

New Micro diaphragm pumps, 100% leak free, oil fee and contamination free sampling. Available with corrosion resistant and heated head options. Motors available with IP20 115/230V, 50/60HZ operation, Brushless Dc and air driven options. Most items available from stock for immediate delivery!!

The FAULHABER Group introduces the 2232-SR DC Micromotors
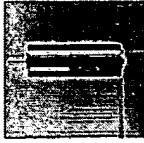
Introducing the 2232 ... SR series – the FAULHABER Group has added another powerful drive to its range of DC micromotors with integrated encoder. The motor, featuring a diameter of 22 mm, a length of 32 mm and an NdFeB magnet, boasts an exceptionally high constant torque of 10 mNm. With an output power of over 9 watts, it is particularly well suited to demanding applica ...

MicroMo
Electronics Inc.
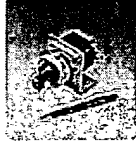
Sub-Microliter Dispensing!

"From 500 Nanoliters to 5 Microliters" Fluid Metering, Inc. of Syosset, NY introduces the NEW Model SMTRH for precision ultra-low volume sub-microliter dispensing making it ideal for medical diagnostic, biomedical, and analytical instrumentation. The SMTRH utilizes FMI's patented CeramPump® valveless piston pumping principle and has a fluid path of zirconium and cera ...

FLUID Metering Inc.

Polymer MEMS for Micro Fluid Delivery Systems

Ellis Meng and Yu-Chong Tai

Department of Electrical Engineering
California Institute of Technology
M/C 136-93, Pasadena, CA 91126, USA

Introduction

Polymer materials for microelectromechanical systems (MEMS) technology have been gaining in popularity to meet biocompatibility requirements of biological and chemical applications. Silicone rubbers have been explored extensively by many in a wide range of applications from cell sorting [1] to capillary electrophoresis [2]. However, the major drawback of using this material is the incompatibility with other microfabrication techniques and processes. Parylenes have long been used in integrated circuits and as a printed circuit board coating for its excellent electrical and mechanical properties. Much attention has now been shifted to the fabrication of biocompatible devices using parylene as a structural material. Neuroscientists have taken advantage of the biocompatibility of parylene in the form of coatings on implantable microelectrodes [3]. In addition, parylene is compatible with microfabrication techniques and forms a conformal, pinhole-free coating at room temperature.

A miniature prototype fluid delivery system incorporating polymers as structural materials is presented here using a micropump as the fluid actuator, a thermal flow sensor as a fluidic control device, and micromachined couplers as fluidic interconnects. This type of system is important in the development of micro-dispensers for lab-on-a-chip.

Experimental

Parylene Check-Valved Diaphragm Pump. Various micro mechanical diaphragm pumps have been designed to achieve the maximum flow rate possible using microfabricated parts. Typically, microfabricated pumps operate with maximum flow rates in the nL/min-µL/min range [4]. Flow rectification in these pumps was accomplished by using high-flow parylene check valves. These one-way valves consist of thin film parylene valve caps that are tethered over an orifice to a silicon substrate. Flow is only permitted when the valve cap experiences forward flow across the valve cap and seat. Operation of such a valve is shown in **Figure 1**. It has been shown that such a valve is capable of providing a four-fold improvement in flow handling capability when compared to similar microfabricated valves [5]. Bossed silicone membranes and gaskets were also used as pump components. Device fabrication details are given in [6] and additional information can be found in [7]. Using this pump, it is possible to achieve flow rates of 13 mL/min. **Figure 2** shows an assembled pump and 3D cross sectional view of a pump assembly.
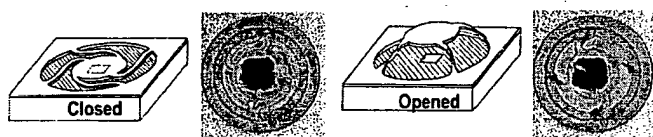

Figure 1. Diagrams and photos showing parylene check valve operations in both closed and opened modes.
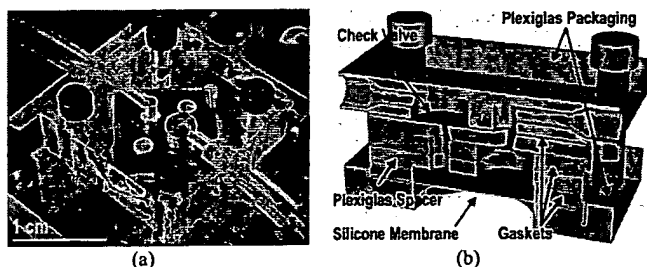

Figure 2. (a) Top view of an assembled micro check-valved diaphragm pump and (b) 3D schematic showing pump components.

Parylene Thermal Flow Sensing Array. Flow sensors based on thermal operating principles have long been popular for their ease of use and fabrication. Sensors for use with biological applications, however, require low operating temperatures and biocompatibility. A thermal flow sensing array constructed of parylene and platinum has been demonstrated [8] and satisfies both of these requirements. Various views of the sensor are seen in **Figure 3** and **Figure 4**. This device operates based on the flow rate dependent convective heat transfer from a heated sensing element to passing fluid. In addition, the sensor is capable of multiple modes of operation and can sense flows as low as 0.5 µL/min. In one operating mode, called time-of-flight, flow rate is measured by tracking a heat pulse applied to a heater at a sensor downstream. The detected signal measured in terms of resistance change over time is shown for various flow rates in **Figure 5**. The characteristic response shows that as the flow rate increases, the time at which the peak signal is detected, or "top time," decreases. Flow rates are set and supplied by a precision syringe pump (KD Scientific Inc. Model KDS 100) fitted with precision syringes (Hamilton Company 1700 Series GASTIGHT syringes).

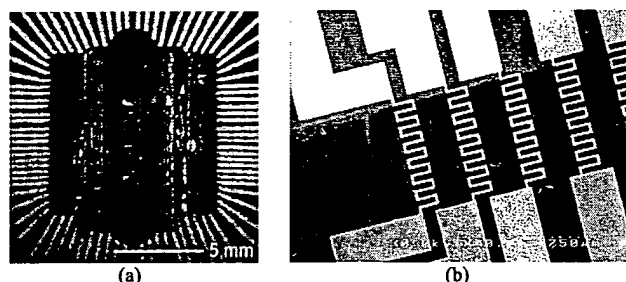**Figure 3.** (a) Top view of packaged flow sensing array and (b) SEM of platinum flow sensing elements suspended on a parylene membrane.
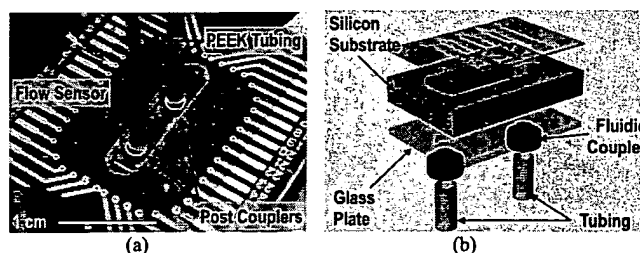

Figure 4. (a) Backside of packaged flow sensing array showing microfluidic couplers and (b) exploded 3D drawing of flow sensor components and assembly.
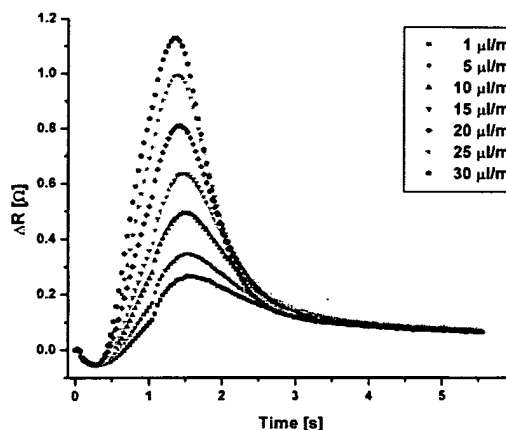

Figure 5. Sensor response at various flow rates measured in terms of resistance change over time for time-of-flight operation.

Microfluidic Couplers. Microfluidic devices require both fluidic and electrical interfaces with the outside world. While electrical interconnects are well developed, the problem of making fluidic connections to microfluidic devices with μm- or mm-scale orifices is still not completely solved. The fluidic coupling approach used here is to connect fluidic devices to the external environment using micromachined silicon and polymer couplers [9]. Several types of micromachined fluidic couplers are shown in **Figure 6**. These couplers are designed to work with conventional PEEK and fused silica capillary tubing and are constructed of silicon or polyolefin. These couplers are extremely robust and support pressures up to 10^4 kPa (1500 psi).
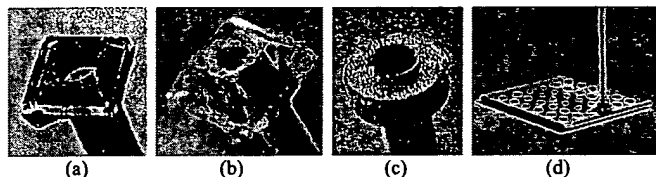

Figure 6. Three types of couplers: (a) silicon bulk, (b) polymer molded, (c) and silicon post couplers; and (d) a silicon post coupler with fused silica tubing attached to a microfluidic chip.

System Assembly. The discrete microfluidic devices previously presented were joined using micromachined couplers to create a micro fluid delivery system. Here, the check-valved diaphragm pump serves as a fluid actuator and is connected to a downstream flow sensing array using silicon post couplers and PEEK tubing. The flow sensing elements are connected to a data acquisition unit (Hewlett Packard HP34970). Filtered deionized water was pumped through the system and out through a calibrated pipette where the flow rate is measured by a stop watch. The flow sensor was operated in time of flight mode using a 3 volt pulse with 1 second duration. While closed loop control is possible, it is not implemented for simplicity. A schematic diagram detailing the system components and data acquisition setup is shown in **Figure 7**.
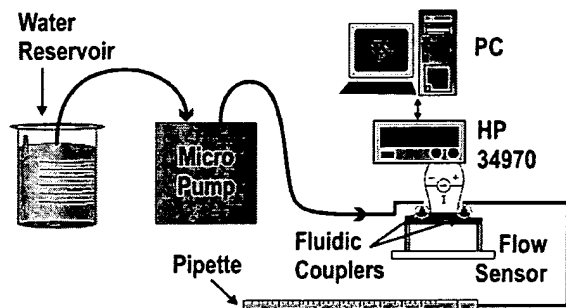

Figure 7. Schematic diagram of flow delivery system layout and experimental testing setup.

Results and Discussion

A working microfluidic system composed of mostly polymer components has been successfully assembled and tested. Performance os the system can be seen in **Figure 8** which shows the sensor output in time-of-flight mode for flow driven by the micro diaphragm pump. The 0 Hz trace corresponds to 0 μL/min flow and the 10 Hz trace corresponds to a flow rate of 46 μL/min. The frequency refers to the actuation frequency of the micro pump actuator. Values for top times and peak response are indicated. Compared to typical time-of-flight sensor response curves, there is noticeable roughness in the 10 Hz signal. This is attributed to the non-continuous flow produced by the reciprocating actuator in the diaphragm pump. In a typical pumping cycle, only the pump mode contributes to the overall flow while the supply mode replenishes fluid in the pump in preparation for the next pumping cycle. At lower flow rates, and thus lower actuation frequencies, this pulsed flow effect on the sensor output is much more pronounced [7].

This system demonstrates the feasibility and usefulness of an integrated dosing system. A further refinement to this system would be to scale the entire system down to chip level. This is ideal in applications where small flow rates (μL/min to nL/min) are desired. Parylene-based MEMS technology

can be used to make reservoirs, valves, pumps, and other components all within a surface micromachined channel for performing various fluidic functions. This multi-layer parylene technique has been demonstrated in [10] in which a continuous flow micro fluid delivery system was fabricated.
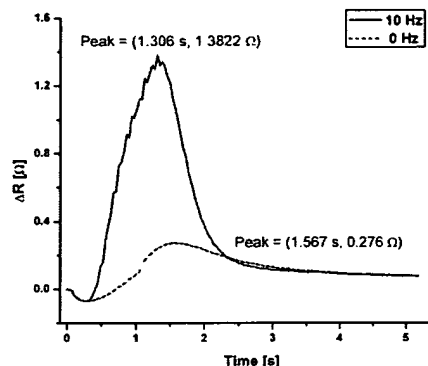

**Figure 8.** Flow sensor response to pumped fluid flow in time-of-flight operation.

Conclusions

Polymer materials have been readily incorporated into MEMS devices. Various polymer components such as parylene check valves, silicone membranes, and parylene supported sensors have been fabricated using MEMS technology. In turn, these discrete devices have been successfully integrated into a functional microfluidic system capable of delivery fluids in the mL/min to μL/min range. Integrated approaches to making completely functional surface-micromachined parylene based fluidic systems have been proven feasible and are being investigated.

References
(1) Fu, A.Y., C. Spence, A. Scherer, F.H. Arnold, and S.R. Quake *Nature Biotechnology* **1999**, 17(11), 1109.
(2) Effenhauser, C.S., G.J.M. Bruin, A. Paulus, and M. Ehrat *Analytical Chemistry* **1997**, 69(17), 3451.
(3) Schmidt, E.M., J.S. McIntosh, and M.J. Bak *Medical and Biological Engineering and Computing* **1988**, 26, 96.
(4) Nguyen, N.-T. and S.T. Werely, *Fundamentals and Applications of Microfluidics*. **2002**: Artech House, Inc.
(5) Wang, X.-Q., Q. Lin, and Y.-C. Tai, *A Parylene Micro Check Valve*, in *MEMS '99*. **1999**: Orlando, FL. p. 177.
(6) Meng, E., X.-Q. Wang, H. Mak, and Y.-C. Tai, *A Check-Valved Silicone Diaphragm Pump*, in *MEMS 2000*. **2000**: Miyazaki, Japan.
(7) Meng, E., *MEMS Technology and Devices for a Micro Fluid Dosing System*, Ph.D. Thesis in *Electrical Engineering*. **2003**, California Institute of Technology: Pasadena, CA.
(8) Meng, E. and Y.-C. Tai, *A Parylene MEMS Flow Sensing Array*, in *Transducers 2003*. **2003**: Boston, MA.
(9) Meng, E., S. Wu, and Y.-C. Tai *Fresenius Journal of Analytical Chemistry* **2001**, 371(2), 270.
(10) Xie, J., J. Shih, and Y.-C. Tai, *Integrated Surface-Micromachined Mass Flow Controller*, in *MEMS '03*. **2003**: Kyoto, Japan.
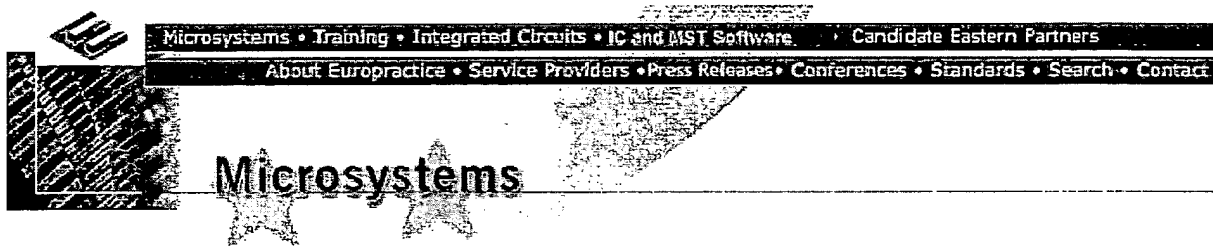
Microsystems/Development/Microfluidic Devices/Pumps

Markets: Environmental. Instrumentation & Process Control. Medical.

Ultrasonic Driven Minipump

Low dimensions, high performance minipump driven by ultrasonic minimotorstems &
down-hole drilling.

Self-priming, reversible functioning, no maintenance.

The applications of this pump should be addressed in every fields where a precise
volume of small quantity of liquids are requested, including abrasive, corrosive, and
aggressive liquids and in general where contamination must be voided:

- pharmaceutical and biotechnology industry,
- chemical industry
- cosmetic industry
- alimentary industry
- water treatment
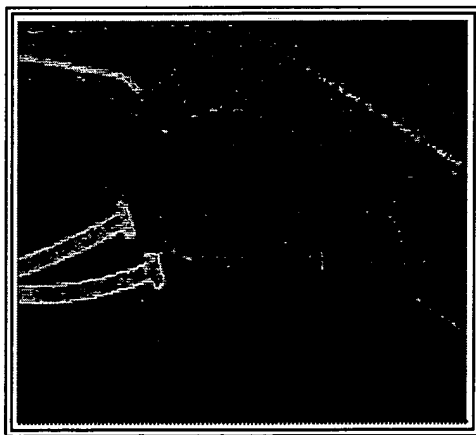
For further information download the data sheet in PDF

Contacts:

General Service Provider Contact
Prof. Paolo Dario,
Scuola Superiore Sant'Anna
Tel: +39 050 883400

E-mail: dario@arts.sssup.it
Web: http://www.mitech.sssup.it/

Specific Service Provider Contact for this Activity
Nicodemo Funaro,
Scuola Superiore Sant'Anna
Tel: +39 050 883400
E-mail: n.funaro@mail-arts.sssup.it
Web: http://www.mitech.sssup.it/

OR

Bernardo Magnani, Pont-Tech
Tel: +39 0587 296404
E-mail: magnani@pont-tech.it
Web: http://www.pont-tech.it/

Ultrasonic Driven Minipump

Technical specification:

1. External dimension (mm): ϕ 34 x 33
2. Suction head: 8 m H_2O
3. Delivery pressure: 0.8 bar
4. Weight: 65 gr
5. Delivery rate: 1 - 80 ml/min

Additional characteristics:

- Self- priming
- Reversible functioning
- Low maintenance

Datasheet of US motor:

- Input voltage: 100 VRMS
- Nominal torque: 0.04 Nm
- Nominal working power: 1 W
- Nominal speed: 250 rpm
- Maximum torque: 0.09 Nm
- Response time: 1 ms
- Direction of rotation: CW/CCW
- Operative life: 1000 ore
- Working temperature: -10÷+50 °C

Datasheet of motor driver:

- Input voltage: 12 V DC ± 10 %
- Input current: 1 A
- Output voltage: 100 VRMS
- Operations form control panel: Start, CW/CCW, speed variation
- Weight: 180 g

SIMULATION OF MEMS PIEZOELECTRIC MICROPUMP FOR BIOMEDICAL APPLICATIONS

Ulises F. González, Ph.D.
ALGOR, Inc.

Walied A. Moussa, Ph.D.
University of Alberta

Abstract

In this study, we demonstrate the usefulness of Finite Element Analysis (FEA) and simulation techniques in the design of MEMS micropumps. Such pumps provide for the handling of milliliter-scaled fluid volumes desired in many lab-on-a-chip chemical and biomedical applications. This worl is focused on a micropump driven by the piezoelectric effect, which in turn invokes the dominant resonance behavior. Because the design of the device is the emphasis of this study, the model wa: originated in CAD and includes the fine-scale geometric details commonly encountered in a wide variety of micropumps. The model considered in this study is a rectangular micropump with a piezoelectrically actuated diaphragm on its top and two valves on its bottom. The mechanical efficiency of the pump hinges on using resonance to generate sufficient motion of the diaphragm. Mechanical Event Simulation (MES) commercial software from ALGOR was utilized to simulate this motion, and thus provide a method for optimizing the design. The results show that consideration needs to be given to the voltage-driving frequency because of its effect on the pump performance and the stress levels within it.

Introduction

The advent of micro fabrication methods has been used to manufacture a wide range of miniature pumps. These micropumps find their greatest application in chemical and biomedical applications requiring the transport of small, accurately measured liquid quantities. When utilized in chemical applications, micropumps are often a component of a lab-on-a-chip device. Such devices are envisioned as providing for reasonably inexpensive, possibly even disposable, means to conduct laboratory experiments. The same technology is utilized in biomedical applications, where micropumps can be used to administer small amounts of medication at regular time intervals. One recent key application of micropumps is to provide a means to deliver insulin to many diabetic patients, thus providing an alternative to injections. Such types of micropumps can be programme to administer insulin at a constant rate throughout the day, thus eliminating any surges or deficits the drug in the patient's bloodstream. This is a highly desirable feature, which could certainly have significant impact on the multi-million, worldwide market for insulin delivery systems. Obviously, other medical markets exist for micropumps, with cancer treatments being the most prominent.

The strict performance requirements of medical devices call out for highly reliable micropump designs. There is an extensive amount of research into the design of micropumps, ranging from experimental to analytical studies. For example, micropumps utilizing no-moving-parts (NMP) valves, driven by a piezoelectric element bonded to a flexible membrane have been developed by ; number of research groups such as S. F. Bart et al. [1], Smits [2], Forster et al. [3], Gerlach and Wurmus [4], Olsson et al. [5] and Das et al [6]. Recently, pump heads of over 7 m of H_2O have been achieved by Olsson et al. [7]. However, no systematic methods have been reported that predict pump performance and guide the design of optimally performing pumps. Some of these pumps are actuated by a piezoelectric disk bonded to a membrane covering the pump chamber. Tc achieve high performance, these pumps are operated at a system resonance. A simplified theoretical analysis of resonant behavior was discussed by Olsson et al. [8]. Also, Mu et al. [9] designed a micropump based on a new valveless pump principle using nozzle or diffuser

components, which even at miniature length scales, result in accurate flow volume control and higl reliability. Recently, Maillefer et al. [10] developed a low-cost, high-performance silicon micropum| for a disposable drug delivery system. Another high frequency, high flow rate, piezoelectrically driven MEMS micropump was manufactured and tested by Li et al [11]. On the analysis side, Eder€ [12] presented a method to describe the behavior of a pump that utilizes a piezoelectric paddle. In this pump, mechanical and fluidic mechanisms are combined in a one mass oscillator model with fluidic damping. With that model, it is possible to simulate the complete droplet ejection process. I a similar work, Nedelcu and Moagar-Poladian [13] modeled the flow of viscous liquids and describe a method to improve the piezoelectric micropump efficiency.

In this paper, the use of FEA is focused on analyzing the stress levels experienced by a common micropump design. The micropump is driven by a piezoelectric component bonded to a moving diaphragm, which in turn forces fluid through a small chamber. The question is how the stresses caused by the deforming diaphragm will affect the pump effectiveness, durability and, thus, reliability. Certainly, maintaining these stresses as low as practically possible will prolong the working life of the pump.

Theory

The dynamic nature of these pumps prompts us to consider a nonlinear FEA simulation capable of calculating stresses caused by both deformation as well as by inertial effects. One may argue that inertial effects should be insignificant at the length scales associated with micropumps, which tend to be on the order of a few micrometers. However, because of the high oscillation rates achieved b these devices, a proper design should account for inertial effects. A geometric nonlinear analysis is also required because of the relatively large geometric changes experienced by some components within these micropumps. In the micropump presented in this paper (see Figure 1), the diaphragm and valve flaps experience the largest deformation, and thus stresses.

The method of operation of this pump is to use the piezoelectric effect to excite the diaphragm at i first natural frequency. The resulting large-scale motion pumps the fluid through the pump chamber, with the inlet and outlet valves passively undergoing oscillatory movements. The resonai motion of the diaphragm, which is bonded to the piezoelectric component, makes its stresses critic to the design of the micropump.

Resonant actuation is strongly desired to achieve the required performance of many piezoelectrical driven micropumps. The piezoelectric component used in the current work is configured such that i deforms in the planar direction upon the application of a voltage across its thickness. This deformation results in the deflection of the diaphragm. Generally, very high voltages (on the order of thousands of volts) are required to obtain the desired deformation in the diaphragm. This high voltage value is not feasible. One reason is that the Joule heating effect induced by such voltages would result in temperatures too high for most applications, especially those involving biological systems. Two common methods of avoiding the need for the high voltages are (1) to force the system at its primary natural frequency, and (2) to use multi-layered piezoelectric components. These methods are not exclusive of each other, and when properly applied, can yield micropump designs capable of safely producing adequate flow rates.

The Micropump Numerical Model

The micropump analyzed in the current study is based on an actual micropump device manufactur, by the Insititut fur Festkoerpertechnik (IFT) in Munich, Germany (Linnemann et al. [14] and Woias et al. [15]). The overall dimensions of this pump are shown in Figure 1 and are 6000×6000×1000 μm for the length, width and height, respectively. Figure 2 shows an exploded view of this micropump, including the Lead Zirconate Titanate (PZT) piezoelectric component, the thin diaphragm onto which the PZT is bonded, the square pumping chamber, and the two orifices that

serve as channels for the inlet and outlet valves. The square geometry of the pump allows for the use of a square PZT stack, which is easier to manufacture than a corresponding circular multi-layer stack. The entire housing of the pump is composed of Silicon Nitride (Si_3N_4), with the diaphragm having a thickness of 10 μm.

Dynamic Analysis of the Micropump

The primary goal of this study was to develop a procedure to incorporate reliability considerations into the design of micropumps actuated using piezoelectric components. The first important step towards ascertaining the reliability of a pump design is to focus on the stresses experienced by the pump during its operation. Because the focus was to only consider the stresses experienced by the diaphragm, it was possible to avoid incorporating the valve flaps in the analysis. The remaining components of the micropump were included in the study.

As discussed earlier, to achieve the best pumping performance, the calculated stresses were obtained during the micropump resonance operating conditions, which result in the most efficient pumping flow rate. In order to take all of these design considerations into account, three types of FEA analysis were considered in the simulation:

1. Electrostatic analysis to obtain the voltage distribution used to excite the piezoelectric material;
2. Linear modal analysis to determine the excitation frequency for resonance; and
3. Geometric nonlinear transient analysis to determine the stresses.

All three analyses were performed using the commercial FEA software, ALGOR, with the nonlinear transient stress results obtained using Mechanical Event Simulation (MES). Before any of these analyses could take place, an FEA model of the micropump was generated using a Pro/ENGINEER CAD model as input. Three-dimensional, 8-node brick elements were used to describe the solid geometry. The same mesh, which consists of 2744 nodes and 2168 elements, was utilized for all three analyses.

The electrostatic analysis consisted of applying a 200V load on each of the 10 layers of the PZT piezoelectric component. For the sake of completeness, the entire geometric model of the micropump was considered in the electrostatic analysis. The bottom of the micropump was grounded, thus the resulting voltage distribution is approximately zero everywhere except on the PZT component. This voltage distribution was subsequently coupled with a nonlinear transient stre analysis. Before the transient analysis could be performed, a linear modal analysis was conducted determine the natural frequencies of the micropump. Figures 3a through 3e show the resulting mode shapes, and corresponding natural frequencies. The mode shapes in these figures are scaled for the sake of visualization. It is important to note that the modal analysis must include the PZT component because, as it is bonded to the diaphragm, its mass and geometry have a significant effect on the overall dynamic behavior of the pump. The usefulness of the modal analysis will become apparent when the details of the nonlinear transient stress analysis are discussed.

Results and Discussion

The nonlinear transient stress analysis was used to obtain a history of the motion of the diaphragm and the resulting stresses. Resonant behavior was utilized to maximize this motion. Specifically, th load induced by the voltage applied to the piezoelectric component was oscillated at a frequency that maximizes the motion of the diaphragm, but, more importantly, at a frequency that maximize the flow rate through the micropump. From Figures 3a-3e, one can ascertain that exciting the micropump at its 1st natural frequency should result in the most efficient design. Because the oscillating peaks and valleys of the 2nd mode are located nearly above the inlet and outlet, one

could argue that this mode could also produce an efficient design as fluid would easily be transferr from the portion surrounding the inlet to that around the outlet – a type of peristaltic motion. The drawback associated with this mode though is that it does not result in the largest volume change throughout a cycle. Because the 1st mode does fulfill the requirement for greatest volume change, became the primary focus of the nonlinear transient stress analysis.

As mentioned above, the nonlinear transient stress analysis was performed using MES. This tool only requires the input of physical data directly attributable to an actual part or assembly. Typical data include material models and associated constants (material constants are provided in Table 1 and methods of loading and constraining the physical object(s). During the simulated event, the micropump was loaded at a frequency of 118.47 Hz - the 1st mode. The magnitude of the load was obtained from a separate linear static stress analysis in which the voltage distribution was held constant, but nevertheless accounted for the piezoelectric effect. The oscillation in the simulated event can thus be considered equivalent to that resulting from a direct transient analysis involving electrostatic effects. For boundary conditions, the micropump is maintained in place by constrainin its bottom surface to remain fixed.

Figure 4 shows the time history of the vertical displacement of a point on the top of the PZT piezoelectric component. This displacement is directly related to the vertical motion corresponding to the 1st mode. The effect of resonance becomes apparent when one considers the results of the separate linear static stress analysis mentioned above. This linear analysis resulted in a maximum displacement of 8.6 μm. In the transient analysis, which corresponds to the simulated event described above, a dynamic maximum displacement of 96.33 μm is reached after 0.092 seconds. Thus, resonant behavior amplifies the displacement by more than an order of magnitude. As Figure 4 shows, this amplification occurs from the onset of the event. This figure also indicates that the maximum peak value is not maintained once it is reached because of the influence of higher mode: Moreover, the displacement is not symmetric about the vertical direction. This is because the PZT component asymmetry adds stiffness to the diaphragm. These asymmetric characteristics associated with the dynamic characteristics of the micropump diaphragm contribute to the stresse: obtained by the MES analysis.

As expected, the maximum stresses occur near the edge of the diaphragm, as shown in Figure 5, where the largest bending moments exist. Figure 5 shows the maximum stresses obtained in this study. These stresses are obtained at time t = 0.096 seconds, which is slightly shifted from the tin point at which the maximum displacement is obtained, 0.092 seconds. This time shift between the calculated peaks of the stresses and the displacements is related to the influence of the inertial effects of the diaphragm. The nonlinear FEA aspect of MES ensured that the analysis accounted for such dynamic effects. Specifically, these stresses are not just cyclical forms of a static stress distribution – as are the applied voltages. In the mechanical case, when large displacement change are occurring in a reasonably short amount of time, assuming quasi-static conditions can lead to significant inaccuracies. In the case of the micropump, the maximum stress at the time of the maximum displacement is 5125 N/mm^2, 18.4% less than the absolute maximum stress at 0.096 seconds. Under dynamic conditions, inertial effects come into play, which impose the need for a nonlinear FEA solution. Furthermore, nonlinear FEA is always required when geometric nonlinearity is expected due to the large-scale motion occurring as a result of the resonance effect.

Knowing the values of the maximum stresses is only part of the design process of most devices. It important to also consider the sensitivity of the design to certain physical parameters, such as geometric dimensions and the loading mechanism. The focal point of this study was placed on investigating the dynamic behavior of the diaphragm when forced to oscillate within a limited rang of frequencies. Figure 6 shows how the absolute maximum displacement varies significantly within this range, and in particular, in the vicinity of the 1st natural frequency of the diaphragm. It is apparent from this figure that driving this pump near its 1st natural frequency will result in the

maximum vertical motion. Nevertheless, at this same frequency the resulting stresses will also be the highest (see Figure 7). Note how the results plotted in Figures 6 and 7 include all of the first fiv natural frequencies in addition to other values used to demonstrate continuity.

Click here to view an analysis replay of the Mechanical Event Simulation of the micropump.

Conclusions

In the current study, FEA is used to simulate the micropump operating conditions and investigate the design constraints for a displacement micropump actuated with a multi-layer piezoelectric material. In this pump model, the dominating multiphysics were simulated using electrostatics and nonlinear dynamics. A solution strategy coupling both of these analyses is applied using the commercial FEA software, ALGOR. In the time domain, a nonlinear geometric analysis is considere due to the large-scale deformation of the pump diaphragm. In addition, inertial effects are also considered because of their significant impact on the dynamic response of the micropump diaphragm during resonance. The maximum displacement and resulting stresses are calculated within a frequency range that contains the first five modes of the pump diaphragm. In terms of displacement, it is shown that the best performance is achieved when the pump is excited at its 1^s natural frequency. This excitation will induce the maximum stress near the edge of the actuated diaphragm. To assure pump reliability for high cycle fatigue, it is, therefore, necessary to design th pump so that the maximum stress level is kept lower than the stress endurance limit of the diaphragm material. This requirement is vital for many types of micro devices considering the role micropumps play in sustaining the reliability of MEMS for biomedical applications, such as lab-on-a chip devices.

References

1. Bart, S. F., et al., "Microfabricated Electrohydrodynamic Pumps," Sensors and Actuators, A21 23, pp. 193-197, 1990.
2. Smits, J. G., "Piezoelectric Micropump with Three Valves Working Peristaltically," Sensors an Actuators, A21-23, pp. 203-206, 1990.
3. Forster, F., Bardell, R., Afromowitz, M. and Sharma, N., "Design, Fabrication and Testing of Fixed-Valve Micropumps," Proceedings of the ASME Fluids Engineering Division, 1995 IMECE, Vol.234, pp. 39-44, 1995.
4. Gerlach, T. and Wurmus, H., "Working Principle and Performance of the Dynamic Micropump Sensors and Actuators A (Physical), Vol.50, no.1-2, pp. 135-140, 1995.
5. Olsson, A., Enoksson, P., Stemme, G. and Stemme, E., "A Valve-Less Planar Pump in Silicon, The 8th International Conference on Solid-State Sensors and Actuators, and Eurosensors IX. Stockholm, June 25-29, pp. 291-294, 1995.
6. Das, P. K., Bhattacharjee, S. and Moussa, W., "Electrostatic Force Modulation as a Flow Control Mechanism in Microfluidic Devices," International Workshop on System-on-Chip for Real-Time Applications, Banff, Canada, 2002.
7. Olsson, A., Enoksson, P., Stemme, G. and Stemme, E., "An Improved Valve-Less Pump Fabricated Using Deep Reactive Ion Etching," Proceedings of the IEEE, Ninth International Workshop on MEMS, pp. 479-484, 1996.
8. Olsson, A., Stemme, G. and Stemme, E., "A Valve-Less Planar Fluid Pump With Two Pump Chambers," Sensors and Actuators A (Physical), Vol.46-47, pp. 549-556, 1995.
9. Mu, Y. H., Hung, N. P. and Ngoi, K. A., "Simulation and Optimization of a Piezoelectric Micro-pump," Int. Conf. of ASME, Nov. 15-20, Anaheim, California, USA, 1998.
10. Maillefer, D., et al., "A High Performance Silicon Micropump for an Implantable Drug Delivery System," Technical Digest MEMS'99, pp. 541-546, 1999.
11. Li, H. Q., Roberts, D. C., Steyn, J. L., Turner, K. T., Carretero, J. A., Yaglioglu, O., Su, Y.-H., Saggere, L., Hagood, N. W., Spearing, S. M. and Schmidt, M. A., "A high frequency high flow rate piezoelectrically driven MEMS micropump," Proceedings IEEE Solid State Sensors and

Actuators Workshop, Hilton Head, June 2000.

12. Ederer, I., "Modeling of a piezo paddle micropump," Technical Proceedings of the Internation Conference on Modeling and Simulation of Microsystems, 1998.

13. Nedelcu, O. T. and Moagar-Poladian, V., "Modeling of the piezoelectric micropump for improving the working parameters," Technical Proceedings of the International Conference o Modeling and Simulation of Microsystems, 1999.

14. Linnemann, R., Richter, M., Leistner, A. and Woias, P., "A full wafer mounted self-priming an bubble-tolerant piezoelectric silicon micropump," Proc. Actuator '98 Conference, (June 17-19 Bremen, Germany), pp. 78 – 81, 1998.

15. Woias, P., Linnemann, R., Richter, M., Leistner, A. and Hillerich, B., "A silicon micropump wit a high bubble tolerance and self-priming capability," J. Harrison und A. van den Berg (eds.), Micro Total Analysis Systems, Kluwer Academic Publishers, Dordrecht, Boston, London, pp. 383-386, 1998.

Silicon Nitride (Si_3N_4)	
Mass density	3.44×10^{-3} N·s^2/mm^4
Modulus of elasticity	3.04×10^5 N/mm^2
Poisson's ratio	0.24
Lead Zirconate Titanate (PZT)	
Mass density	7.5×10^{-3} N·s^2/mm^4
Polarization direction modulus	2.5×10^4 N/mm^2
Transverse direction modulus	2.5×10^4 N/mm^2
Shear modulus	9.5×10^3 N/mm^2
Poisson's ratio	0.31
Transverse charge coeff. (d31)	4.0×10^{-7} mm/V
Longitudinal charge coeff. (d33)	-1.85×10^{-7} mm/V
Shear charge coeff. (d15)	5.0×10^{-7} mm/V

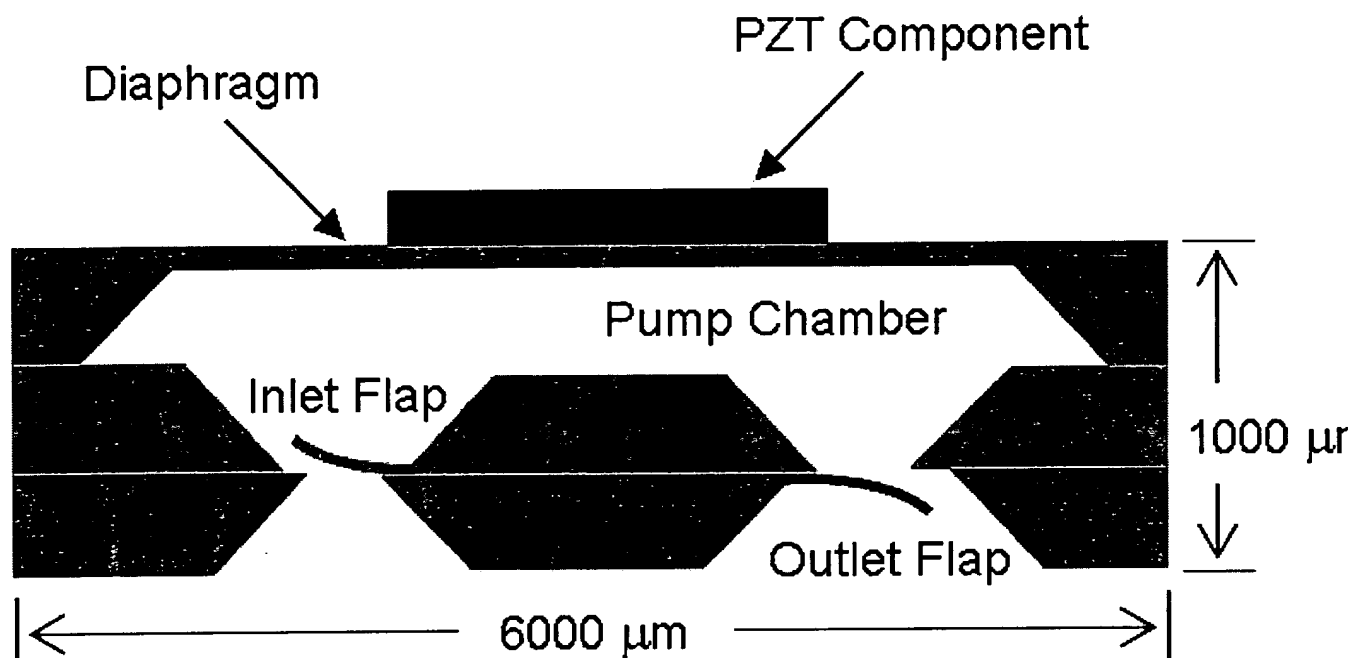**Table 1:** Material constants for material composing micropump.

Figure 1: Sketch of micropump cross-section. Alternating voltage causes the PZT component to expand and contract along the horizontal direction. This induces a bending stress on the diaphragn which in turn pumps the fluid through the chamber.
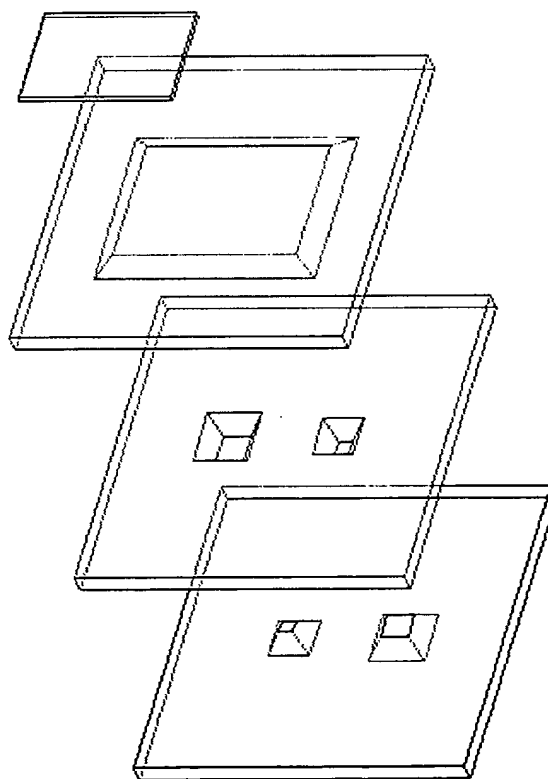

Figure 2: Exploded view of Pro/ENGINEER CAD model used to generate the micropump geometry. Note that the CAD model does not include the flaps associated with the inlet and outlet valves.
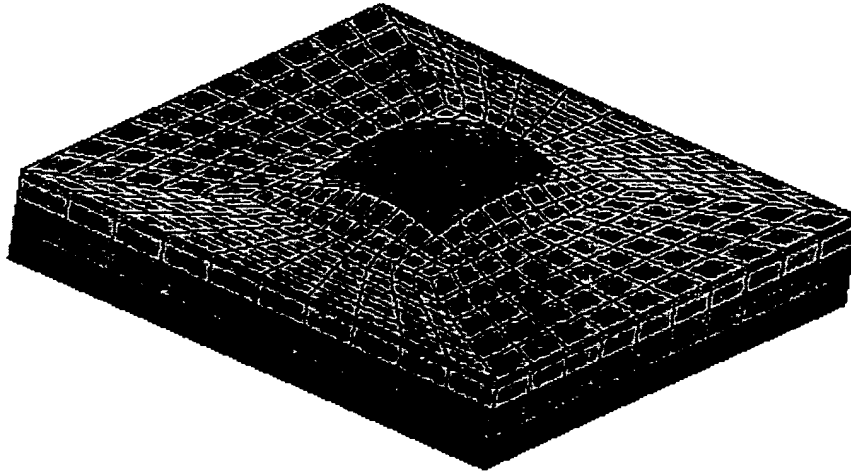
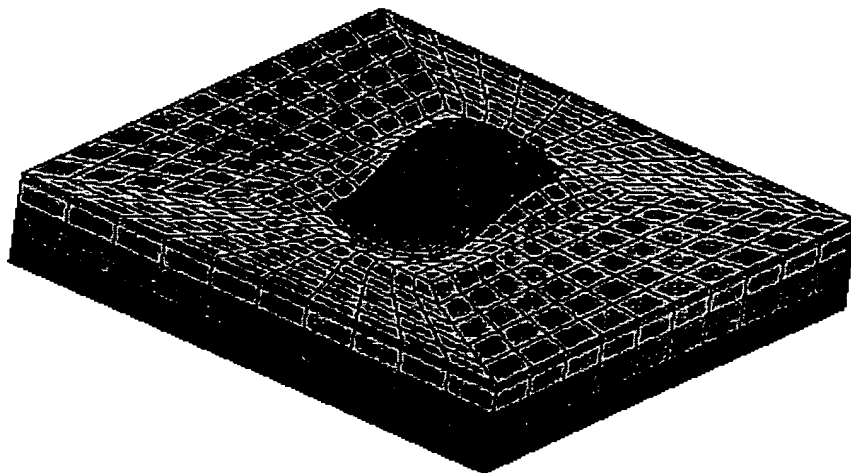**Figure 3a:** 1st mode shape of micropump has a frequency of 118.47 Hz.

Figure 3b: 2nd mode shape of micropump has a frequency of 202.76 Hz.
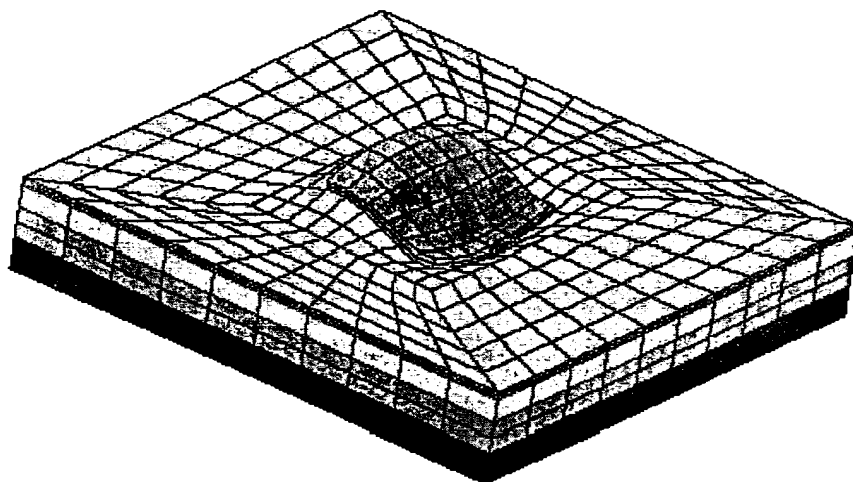
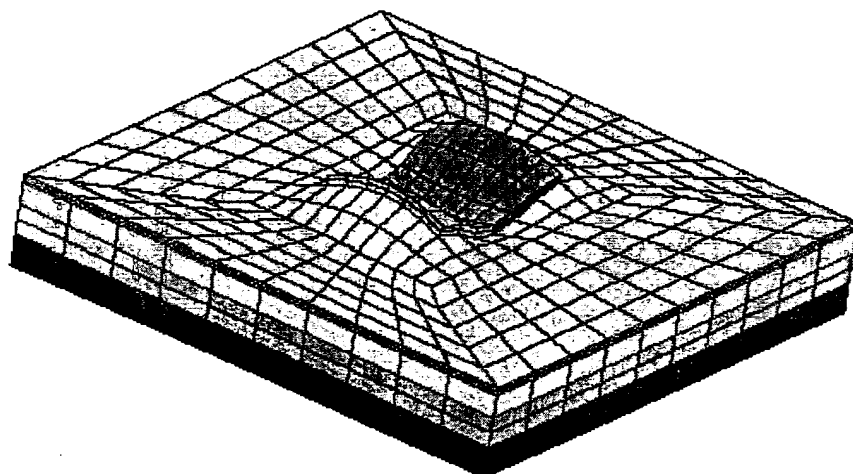**Figure 3c:** 3rd mode shape of micropump has a frequency of 301.00 Hz.

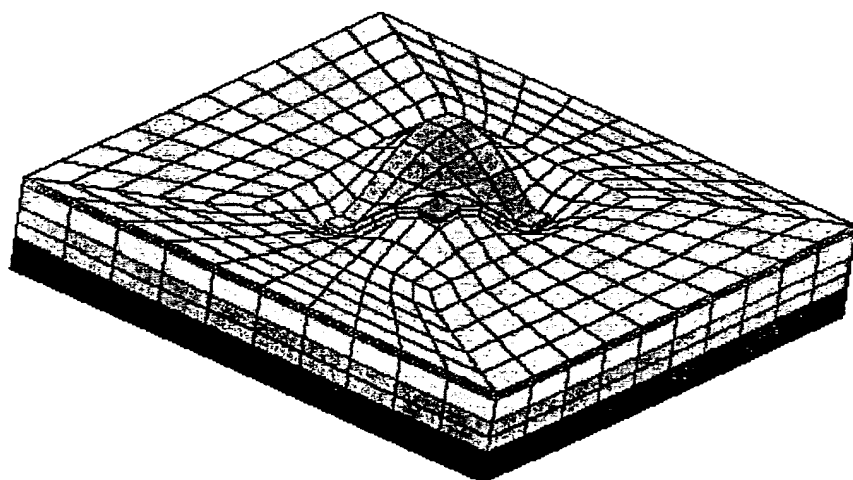**Figure 3d:** 4th mode shape of micropump has a frequency of 349.27 Hz.

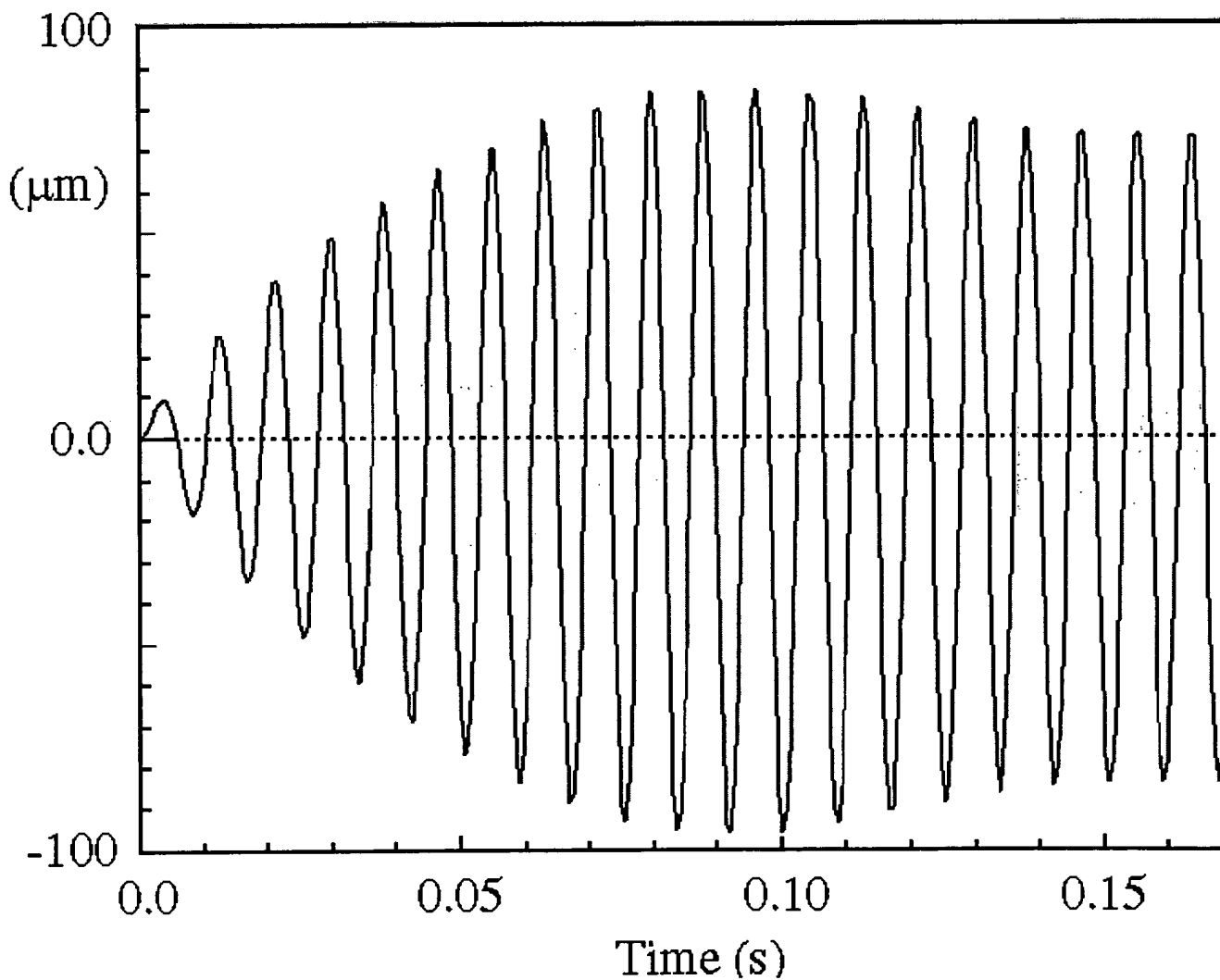**Figure 3e:** 5th mode shape of micropump has a frequency of 381.31 Hz.

Figure 4: Displacement time history of point centered on top of the PZT piezoelectric component
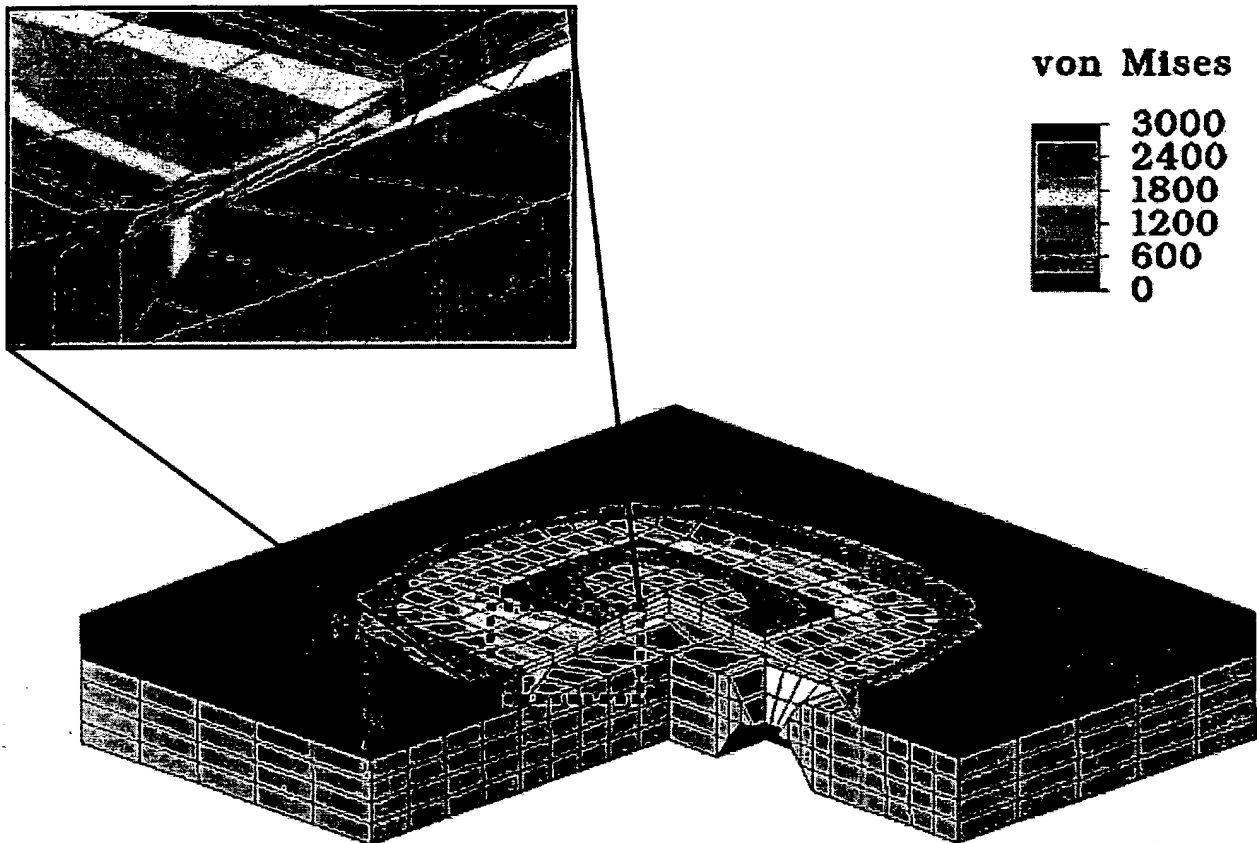
Figure 5: Maximum stresses obtained from MES analysis at time of 0.096 seconds from the beginning of the event. The insert shows the high-stress area, in which stresses are between 3000 and 6283.3 N/mm^2.
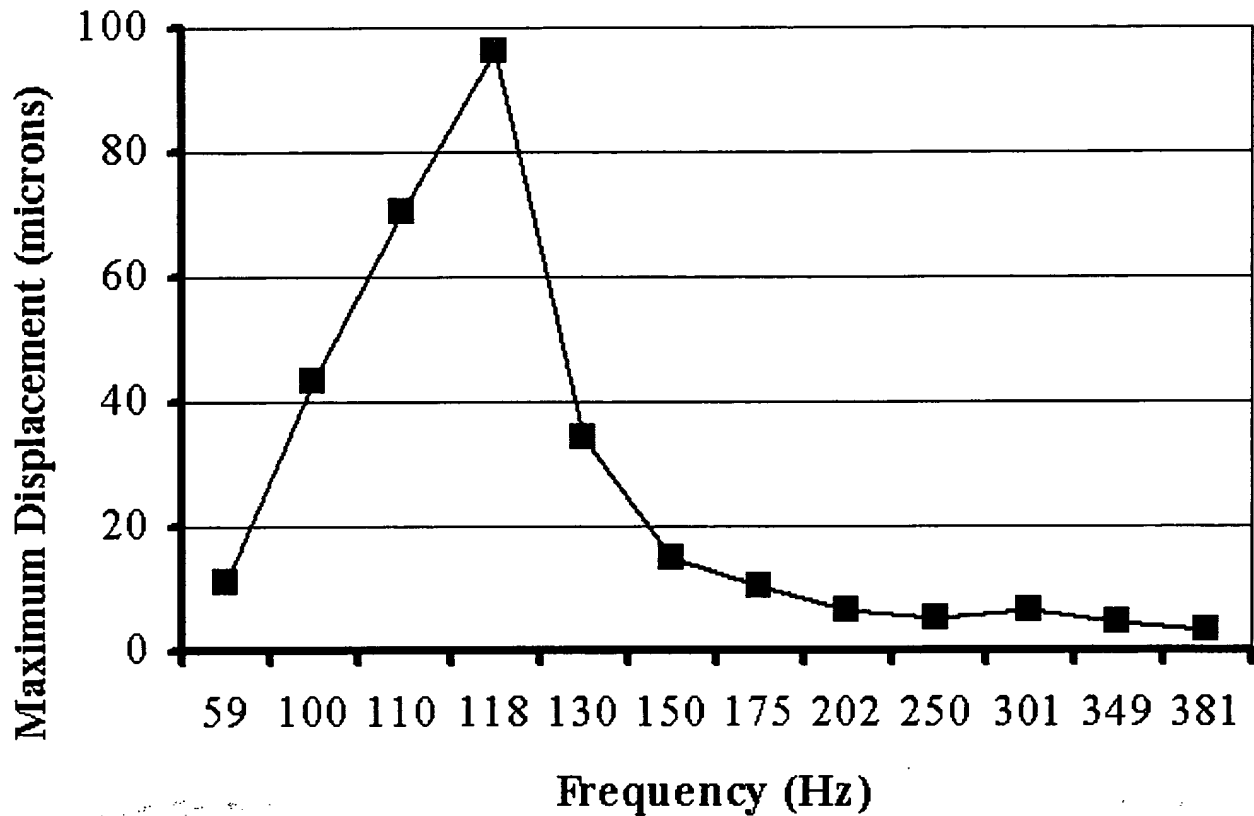
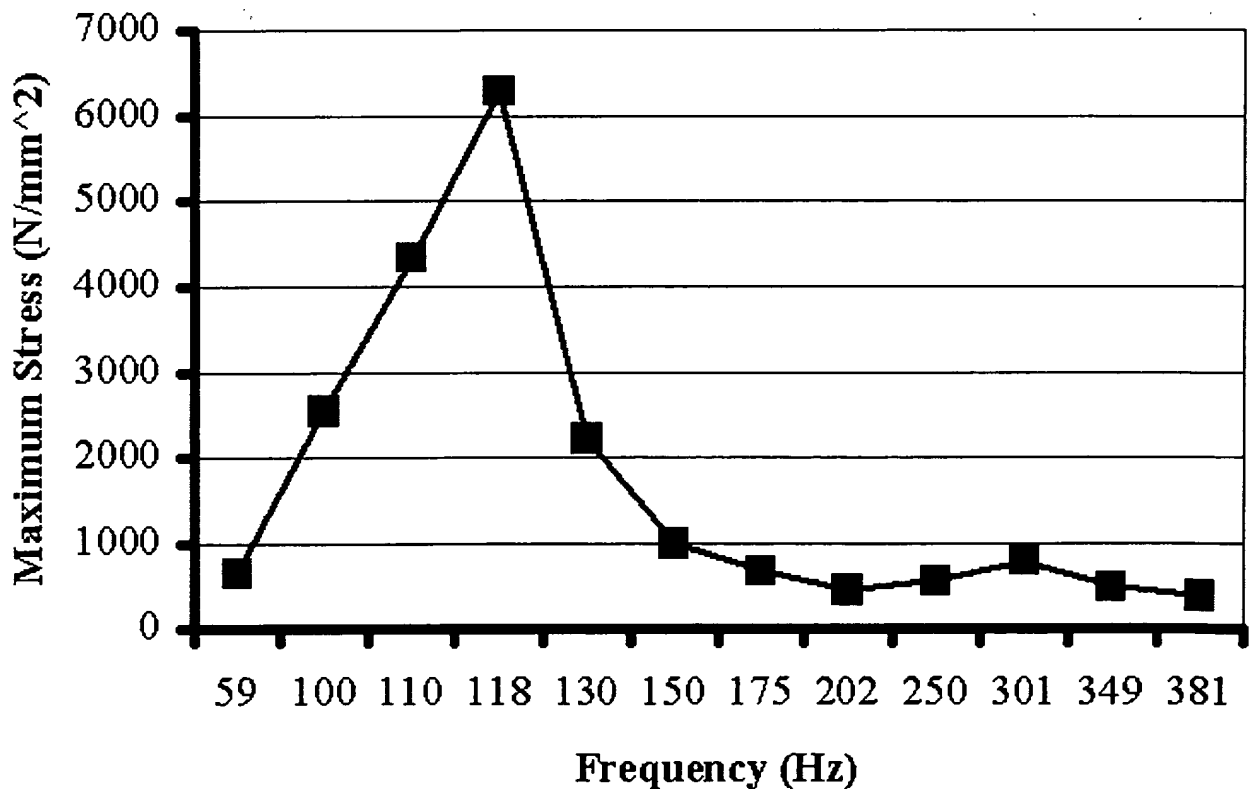**Figure 6:** Maximum displacement as a function of voltage-forcing frequency.

Figure 7: Maximum stress as a function of voltage-forcing frequency.

Back

News Story

Ultra-Low Flow Pump utilizes external gear technology.

May 11, 2004 07:47 - Compact micro annular gear pump minimizes pulsations for smooth, constant flow. It helps conserve valuable liquids such as flavorings, reagents, solvents, inks, dyes, and cleaning agents. For maximum dosage accuracy, rotors provide tight flow rate control, even at differential pressures to 1,160 psi. They allow pump to dispense volumes down to 0.5 µl and handle flow rates from 0.3–288 ml/min with accuracies within ±1%.

Company web site

Press Release

Miniature High Pressure Ultra-Low Flow Pumps

Micropump® introduces a new line of high-pressure micro annular gear pumps offering you greater flexibility and ease in equipment integration. Because of their incredibly compact size and lower mass, you can now place these pumps anywhere within a piece of equipment.

Offering precise and accurate fluid delivery, these new pumps help you conserve your valuable liquids, including flavorings, reagents, solvents, inks, dyes and cleaning agents. For maximum dosage accuracy, the micro annular gear pumps feature high precision rotors that provide tight flow rate control, even at differential pressures as high as 80 bar (1,160 psi). These rotors allow the pumps to dispense volumes as small as 0.5 microliters and handle flow rates from 0.3 to 288 ml/min, with accuracies within +/- 1%.

In addition, the pumps use external gear technology that keeps pulsations to a minimum. This provides the smooth, constant flow necessary in applications such as analytical lab instruments, medical diagnostics, fuel cell and micro reaction technology, chemical processing, biotechnology and other critical application processes.

For more than 40 years, Micropump has led the fluid handling industry in the development of miniature pumps and systems for OEM and industrial applications. Micropump utilizes Kaizen, Lean Manufacturing and Six Sigma process improvement strategies to improve quality and increase value in its product. To learn more about Micropump's fluid handling solutions, contact Micropump Inc. by phone (360) 253-2008; fax (360) 253-8294; e-mail info.micropump@idexcorp.com or on the Web at: www.micropump.com/pr.

Contacts:

General Information:
Joe Stupfel
USA
Phone: 360-253-2008
FAX: 360-253-8294

Company Information:
Name: Micropump, Inc., A Unit Of IDEX Corp.
Address: 1402 N.E. 136th Ave.
City: Vancouver
State: WA
ZIP: 98684
Country: USA
Phone: 800-671-6269
FAX: 360-253-8294
http://www.micropump.com

Online Industrial Process Equipment

**High Quality Products - Long-Term Reliability**

Pumps

Check out our complete line of pump products. These products are selected with the end-user and the OEM in mind. Our peristaltic pumps are some of the smallest pumps on the market. Enjoy the benefits of peristaltic pumps in your application without the high price. Select one of our other pumps for your specialized application.
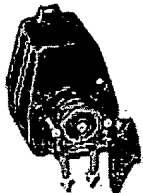
PERISTALTIC PUMPS

SP100 Micro Pump - Small, compact design is among the smallest in the market. Flow rates from 0.4 to 16 ml/min. Select from ac or dc motors.
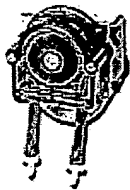
SP200 Mini Pump - Designed to deliver slightly higher flow rates than our SP100. Small size is ideal for many applications. Flow rates from 2.1 to 84 ml/min.

SP200CM Cased Pump - SP200 pumps are mounted in a rugged wash-down (IP65) housing. Variable-flow.
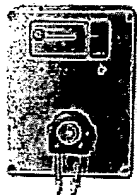
SP200LDS Dispensing Pump - Mount these small dispensing pumps in almost any location to deliver period chemicals, grab samples or to transfer fluids. Built-in timer turns unit on/off over a 24-hr or 7-day period.
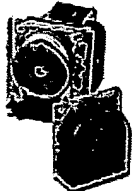
SP300 Compact Pump - The SP300 pumps deliver a high flow rate for their small size. Ideal for sampling or dispensing larger volumes of fluid. Flow rates from 10 to 600 ml/min. (OEM)
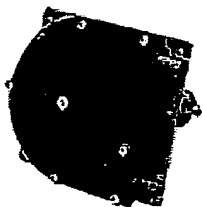
SP400 High Volume Pump - The larger SP400 pumps are designed for industrial flow applications. Design these rugged tubing pumps into your next industrial machine. Flow rates from 0.2 to 4 liters/min.

ProcesSmart.com Home Page

Temperature
Level
Pressure
Flow
Environmental
Instruments
Filtration
Valves
Electrical
Logic
Motion
Controls
TechSmart
Manufacturers
Company Info
Terms of Service
Site Security
Your Privacy
Support
Customers
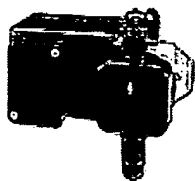Suppliers
News

SEARCH INVENTORY

Search

SEARCH CATALOG

Boolean: AND

Case Insensitive

Search

METERING PUMPS

PM110 Metering Pump - Rugged diaphragm metering pump with adjustable stroke length adjustment for flow control. Economical, continuous-duty pump.

PM150 Metering Pump - Solenoid-driven diaphragm metering pump dual flow control (stroke frequency and stroke length). Chemical resistant, high pressure applications. Select from manual only or manual/remote control models. Integrate easily into pH control system. (OEM)

GEAR PUMPS
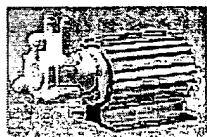
PG10 Gear Pump - Small, compact gear pump with a variety of motor options. Delivers smooth flow. Will not run dry or handle dirty fluids.

OSCILLATING PUMPS

POS10 Pump - Specialty pumps provide fluid transfer at a very affordable price in a small package. Range of voltages available.

VACUUM/PRESSURE PUMP
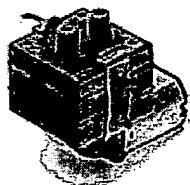
PAD10 Pump - Tiny diaphragm pump is ideal for air and gas sampling. Small Vdc design is ideal for incorporating into air analyzers. Up to 1100cc/min.

All trademarks are the property of their respective owners

- DataQuick, Artisan™ - Advanced Product Technology LLC
- Viton™ - DuPont Dow Elestomers LLC
- Noryl™ - General Electric Company
- Delrin™, Teflon™ - E.I. DuPont Company
- Sta-Pure™ - W.L. Gore
- Norprene™ - Norton Company
- Windows™ - Microsoft Corporation
- SPREETA™ - Texas Instruments

i Home [Air Velocity] [Data Loggers] [Flowmeters] [pH Meters] [Pressure]
[Pumps] [Refractometers]
[Relative Humidity] [RF Transmitters] [Sound Level Meters] [Temperature]
[Tube & Fittings]

Important Notice: By purchasing products from this Site, you acknowledge and agree
that you have read and accept the Terms and Conditions of this online store. For more
information email us at: info@iprocessmart.com

MICROPUMP.

Products
> Pumps
Drives
Accessories

- External Gear
- Piston

- Micro Annular Gear
- Vane

- Peristaltic
- Centrifugal

About Us

Why Micropump

Our Technology

Products

Applications

Tech Tips

Literature

Find Distributor

What's New

Search
[   ] [Go]

Distributor Access

IDEX CORPORATION

Micro Annular Gear Pumps

The compact design of Micropump's micro annular gear pumps offer precise flow rates to 288 ml/min and dispensing volumes as small as 0.25 μl.

Benefits of the micro annular gear pump include:

- Pulseless flow and better than +/- 1% accuracy
- Integrated drive and control to fit easily into OEM equipment
- Long life

The chart below provides a brief preview of all of Micropump's micro annular gear pumps with links to specifications and complete details for each specific series.

If you do not find a pump to match your requirements, please submit your application request and Micropump will be happy to specify a pump for your specific needs.

High Performance	Minimum Flow Rate	Maximum Flow Rate	Maximum Differential Pressure	Maximum Inlet Pressure	Displacement Volume
Model 2900/2905	0.3 ml/min (0.005 gph)	18 ml/min (0.285 gph)	10 bar (145 psi)	5 bar (72.5 psi)	3 μl/rev
Model 4600/4605	1.2 ml/min (0.019 gph)	72 ml/min (1.141 gph)	30 bar (435 psi)	5 bar (72.5 psi)	12 μl/rev
Model 7200/7205	4.8 ml/min (0.076 gph)	288 ml/min (4.564 gph)	80 bar (1160 psi)	5 bar (72.5 psi)	48 μl/rev

Low Pressure	Minimum Flow Rate	Maximum Flow Rate	Maximum Differential Pressure	Maximum Inlet Pressure	Displacement Volume
Model 2521	0.15 ml/min (0.002 gph)	9 ml/min (0.142 gph)	1.5 bar (21.7 psi)	1 bar (14.5 psi)	1.5 μl/rev
Model 2921	0.3 ml/min (0.005 gph)	18 ml/min (0.285 gph)	3 bar (43.5 psi)	1 bar (14.5 psi)	3 μl/rev
Model 4622	1.2 ml/min (0.019 gph)	72 ml/min (1.141 gph)	5 bar (72.5 psi)	1 bar (14.5 psi)	12 μl/rev
Model 7223	4.8 ml/min (0.076 gph)	288 ml/min (4.564 gph)	8 bar (116.0 psi)	1 bar (14.5 psi)	48 μl/rev

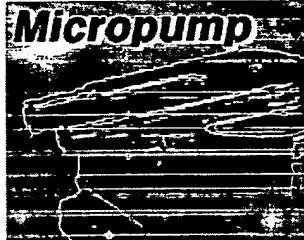*Simple Solutions for a Complex World*™   US: 360.253.2008 / UK: 011.44.148(

Last modified: November
info.micropump@idex
W

Home | product & service | Technology | Corporate Outline | Contact Us   ▶Japanese

Precision Electric Motor & Actuator Questionnaire about our Motor & Actuator

Micropump

Micropump

Proposal and Customizing

Typical Application sample

Products Information

BLDC Motor
AC Induction Motor
Hybrid Stepping Motor
Blower Fan Motor
Geared Motor
Polygon Mirror Scanner Motor
Polygon Mirror Scanner Motor (mini size)
Micro pump

Technology

Lower Noise Technology
Compact/High Efficiency Technology
High Reliability/
    Low Vibration Technology

Ecology Product

Design and Manufacturing with consideration of environmental circumstances

Attention for Questionnaire

Inquiry SPEC. entry sheet
request catalog
Information of Exhibition

Quality &

Developed Micropump for water cooling system

| General Information | Background of Development | Descritiopn and major pec. |Application and Direction of Development in the Future | Patent |
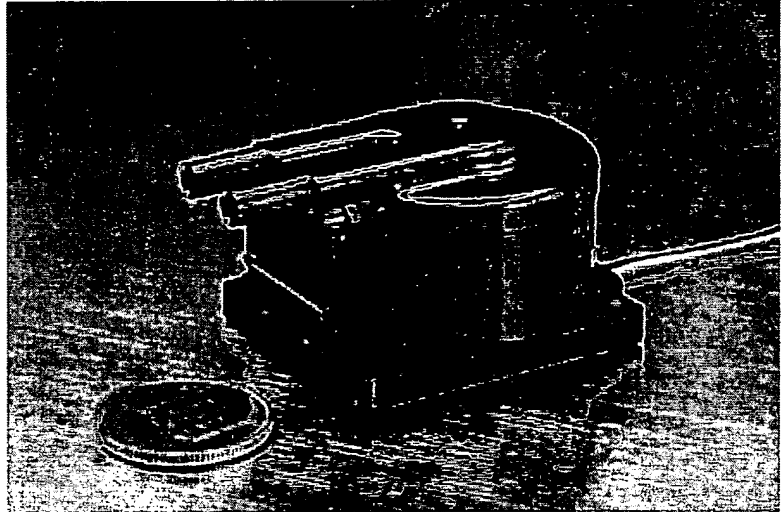
1. General Information

Shinano Kenshi Co., ltd. (President CEO Motoaki Kaneko / Maruko-Machi, Nagano +81-268-1800) who is a market leader of small precision electronic motors has devel high performance, and noiseless water cooling micro pump. Its original structure and control technology can achieve self-restoration performance, high flow, high anti-pre performance, low noise level, and long life currently not seen in the existing micro p at reasonable costs. It is expected use includes a variety of applications such as cooli for PC and other industrial devices. Shinano plans to start manufacturing in June 200

2. Background of Development

Desire for water cooling method according to higher performance of PC

Personal computers (PC - 14 billion machines sold annually world wide) are develop processor speeds with each passing year as demanded by the market. Today, comput process 3×10^9 times a second and more is expected in the future. Process speed of a on the CPU process capability, with higher speed processors requiring higher current that generate higher and higher heating values.
Currently, heat-dissipating axial fans are used with heat sinks for cooling CPUs. To a sufficient cooling performance and lower noise, water cooling system will become n Performance of a water based cooling system for PCs depends on the water flow the generate - a similar method as cooling for an automobile car engine. A compact size water flow is desired. A long life is also highly desirable because maintenance is not practical for the PC user

3. Descritiopn and major pec.

Description   Micropump

Environment

ISO9001
ISO14001
TS16949

Pumping method Electro magnetic driving method, piston pump
Rated pressure   6kPa
Rated flow   400ml/min.
Rated voltage   12V DC
Life   44,000 hours min.

4. Features

A. Electro Magnetic Drive Piston Method as Pump

A self-priming capability enables the self-restoration capability of the pump p(
when an air invasion occurs into the water cooling system. Shinano's pump do
the location of a reserve tank above this pump, and it possible to achieve a fre(
water cooling system.
Good sealed and leakage free.
Because we cannot expect to have a maintenance procedure on a PC cooling s;
important to minimize the loss of coolant. In general, the piston pump has a se
the cylinder and drive transmission so the pump life depends on the seal.
Our piston is driven by magnetic forces thus no slide can achieve a longer seal
performance

B. Low noise

We achieved 20dB (ISO07779) in PC by original electric control method and (
valve, although pump with a piston tends to create noise generally. It is the mc
cooling system for multimedia PCs that are set in a living room

C. Compact , high performance

It achieves 400ml/mimute min. at rated pressure 6kPa. It can fit next generatio
may generate more heat in the future

D. High Anti-Pressure Loss Performance

Due to its original magnetic circuit design, it can generate high pressure to flo\
Even if the coolant route and heat sink jacket form a complex structure, the pu
supply a stable cooling performance compare with a centrifugal pump

5. Application and Direction of Development in the Future

We expect that our micro pump can successfully be used for cooling systems of com
notebook PCs and for industrial devices

6. Patent

We are applying for a patent on our pump's basic, structure and control method

Please contact here
Shinano Kenshi Co.,Ltd.
Electrical Devision
R&D Sales section

1078-0498 Kamimaruko, Maruko-machi, Chiisagata-Gun,
Nagano-Ken, Japan
Phone : +81-(0268)-41-1824
Email->motor@skcj.co.jp

Appendix B

Measurements and Modeling of Two-Phase Flow in Microchannels With Nearly Constant Heat Flux Boundary Conditions

Lian Zhang, Jae-Mo Koo, Linan Jiang, *Member, IEEE*, Mehdi Asheghi, *Member, IEEE*,
Kenneth E. Goodson, *Associate Member, IEEE*, Juan G. Santiago, *Associate Member, IEEE*, and Thomas W. Kenny

Abstract—Two-phase forced convective flow in microchannels is promising for the cooling of integrated circuits. There has been limited research on boiling flow in channels with dimensions below 100 μm, in which bubble formation and flow regimes can differ from those in larger channels. This work develops single and multi-channel experimental structures using plasma-etched silicon with pyrex glass cover, which allow uniform heating and spatially-re-solved thermometry and provide optical access for visualization of boiling regimes. Boiling was observed with less than 5 °C of super-heating in rectangular channels with hydraulic diameters between 25 and 60 μm. The channel wall widths are below 350 μm, which minimizes solid conduction and reduces variations in the heat flux boundary condition. Pressure drop and wall temperature distribu-tion data are consistent with predictions accounting for solid con-duction and homogeneous two-phase convection.   [651]

Index Terms—Heat exchanger, microchannel, two-phase cooling.

I. INTRODUCTION

TWENTY years ago, Tuckerman and Pease [1] predicted that single-phase forced convective cooling in microchan-nels should be feasible for circuit power densities of more than 1000 W/cm^2, and demonstrated a microchannel heat sink that removes 790 W/cm^2 with 71 °C temperature increase at 600 mL/min flow rate. While subsequent research has focused on modeling and optimization of single-phase liquid microchannel heat exchangers [2], [3], the more complicated physics of boiling flow in microchannels has received little attention. Boiling convection is promising because it requires less pumping power than single-phase liquid convection to achieve a given heat sink thermal resistance. Peng *et al.* investigated flow transition and heat transfer in V-shaped microchannels with hydraulic diameters ranging from 200 to 600 μm [4], [5]. Jiang *et al.* studied phase change in diamond-shaped microchannels with hydraulic diameters less than 100 μm [6].

Peles *et al.* proposed a one-dimensional (1-D) flow model with flat evaporation front dividing the liquid and vapor into two distinct domains based on their experiments with 50 to 200 μm hydraulic diameter channels [7]. Other experimental studies have focused on microchannels with larger hydraulic diameters [8]–[10]. However, more research is needed to better understand the behavior of boiling flow regimes in channels with diameters below 100 μm, in particular the impact of the small dimensions on bubble nucleation and the heat transfer coefficient.

In our previous study [11], nucleate boiling was observed in 55 μm hydraulic diameter microchannels. In order to study the phase change as well as heat transfer in microchannels in more detail, we developed single and multichannel devices which are designed to minimize variations in the heat flux boundary con-ditions and preheating of the fluid before entry into the channel. This is achieved by reducing the channel wall thickness and modifying flow entrance geometry. The microchannels are in-tegrated on a bridge structure with a single resistor on one side, which serves as both a heater and a series of thermometers. Channel width ranges from 20 to 50 μm, with 50 to 100 μm in depth, giving a range of 25 to 60 μm hydraulic diameters. A glass slide seals the channels and provides optical access to the internal flow conditions.

We developed simulation models for single and two-phase flow heat transfer using finite volume method. Both homoge-nous flow model and annular flow model were used in two-phase simulation, and the theoretical predictions were compared with experimental results. The homogenous model results are in better agreement with experimental data.

II. DESIGN

Fig. 1 shows the schematic of the test device. The overall dimension is 2 by 6.5 cm. The narrowed bridge design helps to concentrate the heat flux from the resistor to the microchannel region. The outlet is formed in a 3 by 3 mm pad at the end of the channel so that the outlet fluid temperature can be measured with a thermocouple before there is significant heat loss to the surrounding silicon.

Fig. 2 provides more detailed views of the design of the channel region. A 600 -μm wide, 250 -μm deep reservoir is defined at the inlet, with a 2-mm-long entrance region [see Fig. 2(a)]. The entrance region is a part of the microchannel, but not covered by the heater. This design helps to reduce the
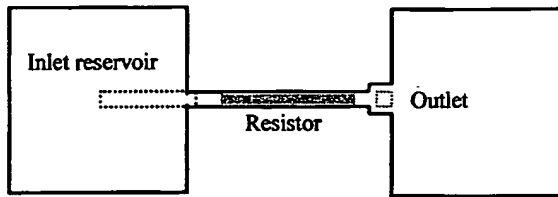
Fig. 1. Schematic of the test device, showing arrangement of inlet and outlet ports and the narrow free standing, instrumented microchannel.
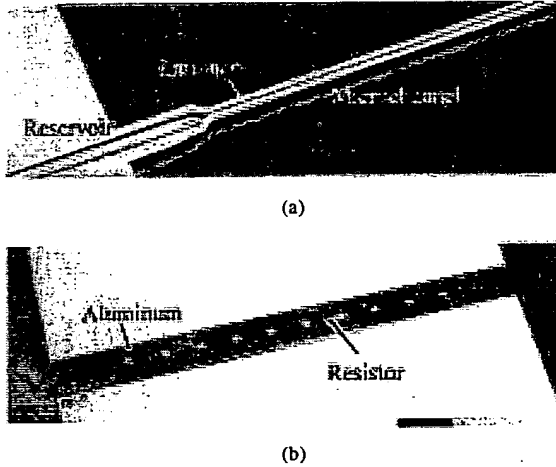

Fig. 2. Close-up views of microchannels and resistors. (a) Single channel design. (b) Resistors on a multichannel design.

TABLE I
STRUCTURAL PARAMETERS

Structure	Dimension
Inlet reservoir	600 μm wide, 250 μm deep, 1 cm long
Bridge	500 μm (single) / 2 mm (multi) wide, 2 cm long
Single-channel design	40-50 μm wide, 50-100 μm deep, 2 cm long
Multi-channel design	20 μm (width) x 50-70 μm (depth) x 40, 40 μm (width) x 100 μm (depth) x 20, 2 cm long
Resistor (heater)	400 μm wide, 1.6 cm long (single) 1 mm wide, 1.8 cm long (multi) 800 Ω (single) and 360 Ω (multi)

preheating of the fluid. There is a similar exit region at the outlet. A single resistor [see Fig. 2(b)] is formed on the back side of the channel by ion implantation to single crystal silicon. The resistor is divided into nine segments and functions as both a heater and nine thermometers in series. When a current is applied to the resistor, the resistance change of individual segments, corresponding to the change of wall temperature, can be measured by recording the voltage across each segment.

In order to study phase-change in microchannels and boiling uniformity across a group of channels, we have developed both single-channel and multichannel test devices. Design parameters are listed in Table I.

III. FABRICATION

For the current micro-scale heat transfer test devices, we have selected 4-inch, N-type, ⟨100⟩ orientation, 400 -μm thick, and
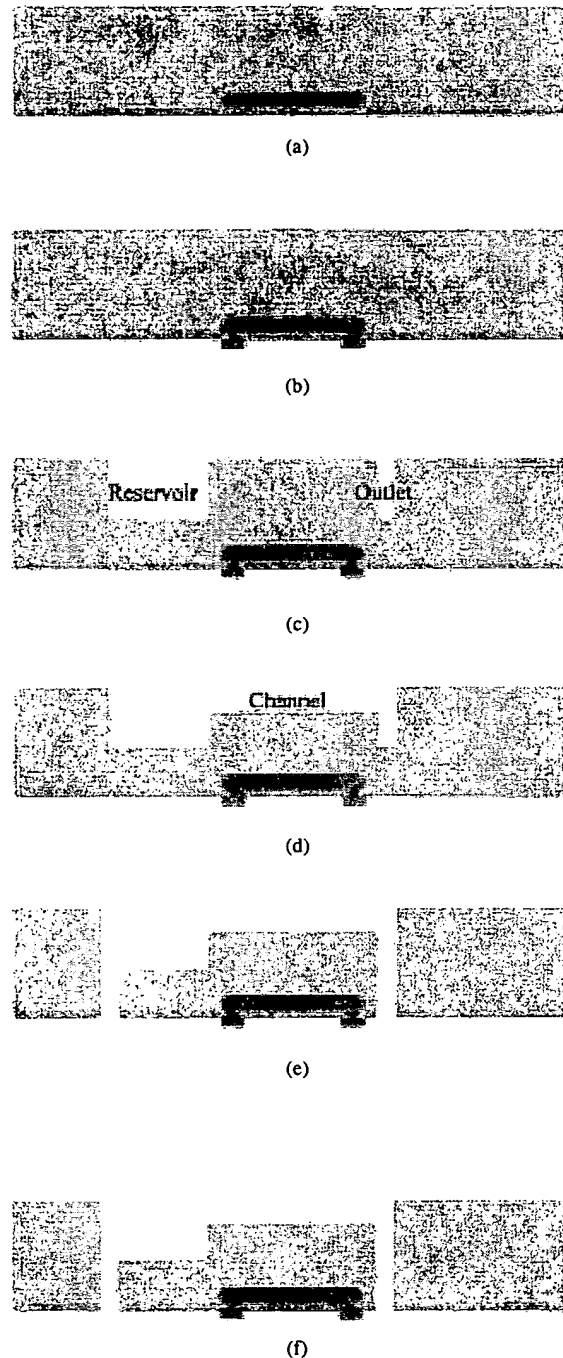
Fig. 3. Schematic of fabrication process. (a) Forming the resistor by ion implantation and anealing. (b) Depositing Al pads as contacts (10 in reality). (c) Front side DRIE etching reservoir and outlet. (d) Etching microchannels. (e) Back side etching inlet/outlet through holes. (f) Schematic of fabrication process.

1000 -Ω/cm resistivity silicon wafers as substrates. As shown in Fig. 3, fabrication process begins with ion implantation to form the resistor on the back side. Boron is implanted to the resistor region at 1e16 ions/cm^2 dose and 40 keV energy, with 1.6 μm photoresist as mask. The dopant is then activated and driven in with 15-min wet oxidation at 1100 °C, followed by a six-hour annealing at 1150 °C. The process forms about 2700 Å silicon dioxide to protect the resistor; with approximately 8 μm

Fig. 4. SEM images of microchannels. (a) A 40 by 100 μm single-channel design. (b) A 40 parallel 40 by 100 μm multichannel design.
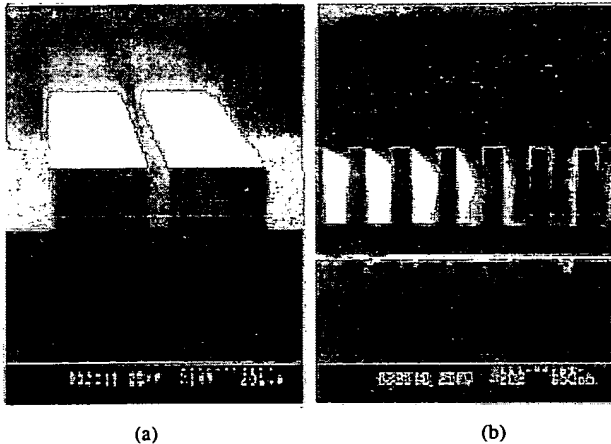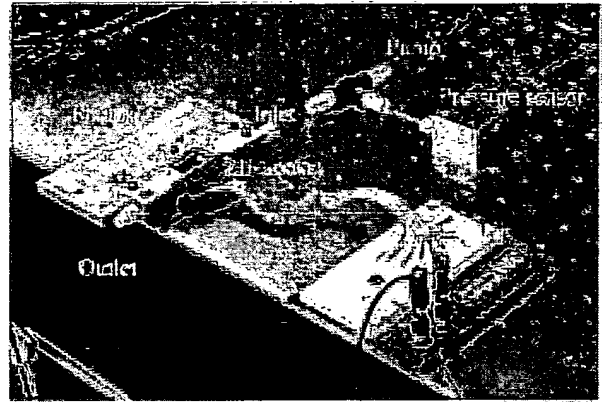

Fig. 5. Photograph of experimental setup, showing microchannel sample mounted in test fixture with electrical connections to the circuit board, and fluidic connections to a syringe pump and a pressure sensor.

junction depth, and 18 $\Omega/\square$ sheet resistance. The deep PN junction with high substrate resistivity can dramatically increase the break-down voltage, which is higher than 100 V in this case.

Next, contact windows are opened through the oxide layer and 99% aluminum with 1% Si is deposited as contacts. Since boron oxide may form during the high-dose annealing process, an argon etch prior to deposition is strongly recommended to form a good contact. After aluminum etch, a freckle etch is performed to remove aluminum freckles from the substrate surface to prevent shorts between contacts. Then the contact is finished by a one-hour forming gas anneal (10% H_2 and 90% N_2) at 400 °C.

The process is then continued with etching the reservoirs and channels from the front side. The 250-μm-deep reservoir and outlet are first DRIE etched into the substrate. Then 7 μm thick photoresist (e.g., SPR220-7 or AZ4620) is used as the channel etching mask, which is thick enough to cover the 250-μm-deep trenches. Channel etching stops at desired depth by a timed etch and inspection, as shown in Fig. 4. Next, the device wafer is bonded to a support wafer with photoresist and etched through. Finally, the device chip is anodically bonded to a prediced Pyrex 7740 piece.

IV. EXPERIMENTAL SETUP

As shown in Fig. 5, the device is clamped in a fixture with an internal O-ring to seal the inlet. A pressure transducer is located at the flow entrance of the fixture. Since the internal flow channels in the fixture are much larger than the microchannels, the pressure drop within the fixture can be neglected. The outlet is open to the air and a 100 -μm-diameter thermocouple is fixed right at the outlet of the microchannel to measure exit water temperature. A constant flow rate syringe pump supplies DI water to the system.

The data acquisition system consists of a laptop computer, a 16-bit, 16-channel PCMCIA A/D card, and signal conditioning circuitry. The system is controlled through LabVIEW G programming, capable of continuously scanning the 12 signals at 1000 Hz frequency.

V. EXPERIMENTAL RESULTS

Various devices were tested under constant flow rates. With these experiments, we aim to verify the pressure variation with heating input through the initiation of boiling. We also aim to measure the wall temperature distribution during phase change as supporting data for our flow model.

Measurement results of two devices are presented here. Device 1 is a 40-channel design, each channel is 20 -μm wide and 70-μm deep (31-μm hydraulic diameter). Device 2 is a 50 -μm wide and 70 -μm deep (58 -μm hydraulic diameter) single-channel design. Both results were measured at 0.1 mL/min constant DI wafer flow rate.

A. Thermometer Calibration

Wall temperature change is indicated by the change in resistance of the thermometers. By recording the applied current and voltage difference across each thermometer, we obtain the resistance, hence the temperature. Temperature-resistance curves of each of the nine thermometers on every single device are individually measured and fitted. The resistances are calibrated by placing the silicon chip in a convection oven with a reference thermocouple, and recording the resistance changes in each segment of the resistor as the temperature is raised through the measurement range of 20 to 140 °C. Fig. 6 gives a typical fitting curve, which includes measurement data from six calibration cycles. In all experimental data in the following figures, the main source of error is uncertainty in the thermometer calibration, which is about ±3 °C.

B. Multichannel Device Measurements

Figs. 7–9 give the pressure and local wall temperature changes against increasing heat power, as well as wall temperature distributions before and after phase change.

In Fig. 7, as we observed before [11], pressure decreases with increasing power during single-phase flow due to the decrease in liquid viscosity with increasing temperature. Just after the onset of boiling, because the density of vapor is much lower than that of water, the local volume flow rate in the channel suddenly increases. The resulting acceleration of the mixture yields a large pressure drop along the channel.
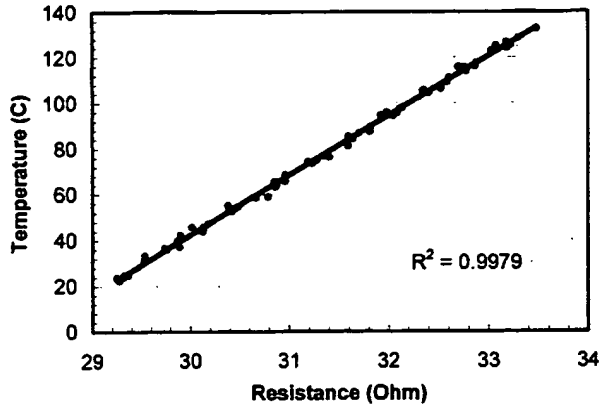
Fig. 6. Thermometer calibration and fitting curve. This figure shows a typical temperature-resistance calibration for one of the resistors in our sample. This figure shows data recorded during six independent calibrations of the same resistor, illustrating repeatability and linearity.
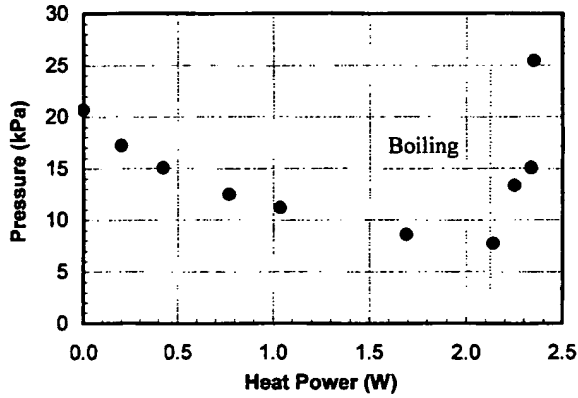

Fig. 9. Wall temperature distributions in a 40-channel device, measured at three heat power levels for a fixed DI water flow rate of 0.1 mL/min. The onset of boiling occurs at 2.14 W heat power.

Fig. 7. Pressure change in a 40-channel device, measured as a function of heat power for a fixed DI water flow rate of 0.1 mL/min.

slight reduction in wall temperature at the initiation of boiling for all of the thermometers. This may be due to the local temperature superheating as a result of nucleation and bubble departure. However, it may also be due to the effect of pressure fluctuations. In work presented elsewhere [12], we show that pressure fluctuations in the microchannel is the main source of small-amplitude resistance changes through a strain effect. Therefore, the onset of these fluctuations in the electrical signals is a very useful indicator of boiling, but the average resistance measurements become more difficult to interpret as temperature measurements. Work is ongoing to understand the relationship between these phenomena in the sensors.

Fig. 9 shows wall temperature distributions at various input power. The parabolic shape results from the conduction losses along the walls into the fluid entrance and exit region.

C. Single-Channel Device Measurements

Figs. 10–12 plot the same measurements performed on a single-channel device. Comparing the results, the pressure curves in Figs. 10 and 7 are similar, except that the onset of boiling in the single channel occurs at a lower heat power (1.32 W) than in multichannels (2.14 W). This is due to the larger heat loss in the multichannel design which will be discussed in the modeling section.

Because of the large change in the pressure distribution along the channel as phase change is occurring, boiling instability could occur if the mass flow rate provided by the pump is coupled with pressure loading. The instability appears as transitions between flow patterns, that is, at some point after boiling begins, the fluid suddenly changes back to liquid phase, then starts boiling again. This cycle usually has a long time period of up to a few minutes. Since the instability affects the flow pattern and heat transfer, the loading capacity should be considered in pump design or selection for microchannel heat exchangers.

Fig. 11 plots the temperature changes of the inlet, outlet and middle point of the channel against increasing heat power. The data indicate no decrease in the wall temperature after the onset of boiling. Once again, it should be emphasized that the uncertainty of the temperature measurements in the two-phase re-
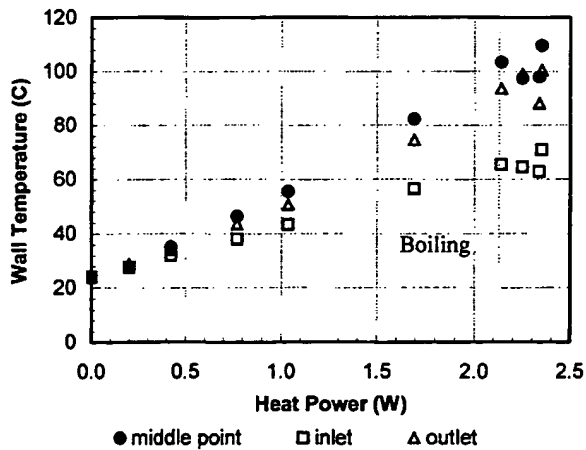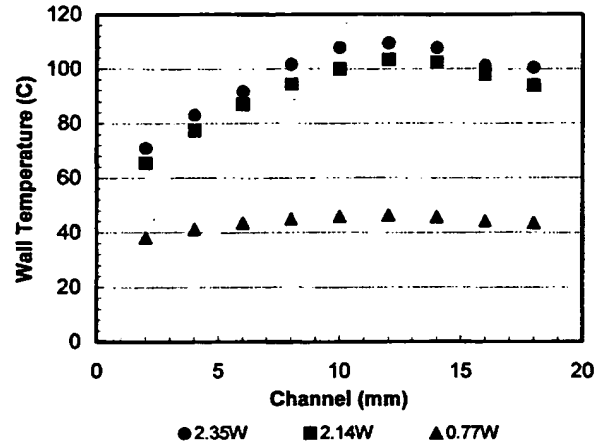

Fig. 8. Local wall temperatures of a 40-channel device, measured as a function of heat power for a fixed DI water flow rate of 0.1 mL/min.

Local wall temperatures are plotted in Fig. 8. Although boiling is quite uniform across the channels, that is, boiling occurs at about the same place in each channel, current and voltage signals at every measurement point begin fluctuating in time after the onset of boiling. The data also indicate a
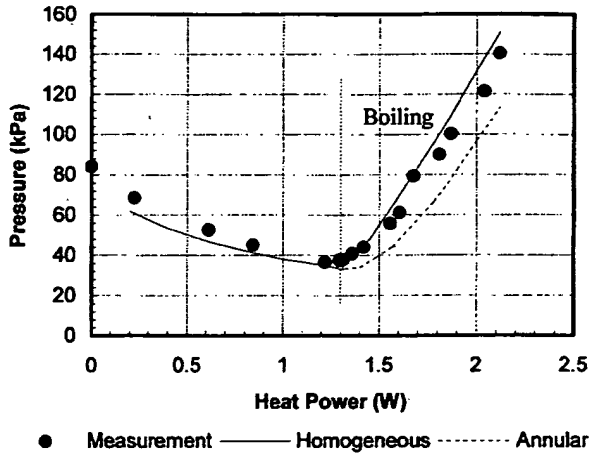
Fig. 10. Measurement and simulations of pressure change in a single-channel device, as a function of heat power for a fixed DI water flow rate of 0.1 mL/min. Both homogeneous and annular flow model simulations are plotted.
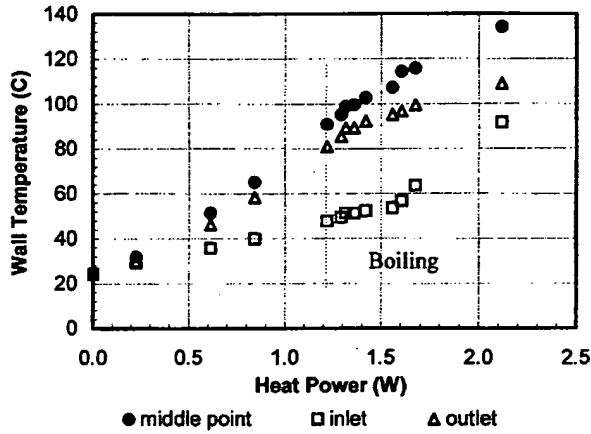

Fig. 11. Local wall temperatures of a single-channel device, measured as a function of heat power for a fixed DI water flow rate of 0.1 mL/min.

gion is increased due to the transient fluctuations in current and voltage signals across the thermometers.

The wall temperature profiles in Fig. 12 are also approximately parabolic, as in the case of the multichannel device. The highest measured wall temperature was 134 °C, which is close to the boiling point of water at the recorded pressure.

Although the phase-change in microchannels is not as stable as in macroscale channels, all our experiments show that nucleation and small bubble growth occur in plasma etched microchannels under 60 μm in hydraulic diameter. No surface condition-induced superheating was measured in these channels. Optical microscopy indicates that the two-phase microchannel flow is mostly annular flow with a very thin layer of liquid. Typical bubbly and plug flow observed in macroscopic channels are absent in these microchannels.

VI. MODELING

The model integrates macroscopic thermal resistances for the test system with microscopic finite volumes for internal microchannel flow. Heat distribution is taken care of in the thermal circuit model, which predicts the fraction of heat carried away
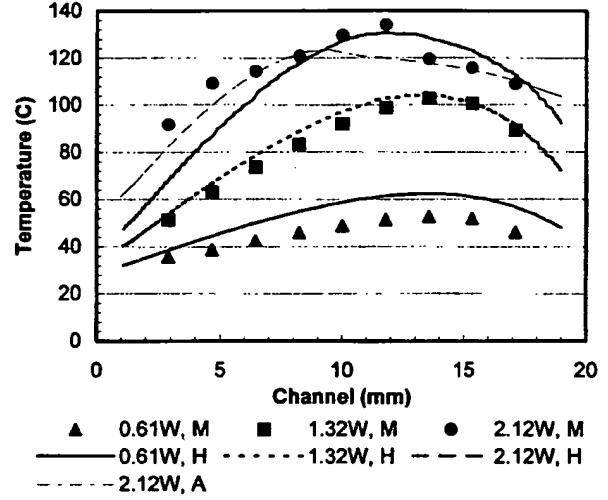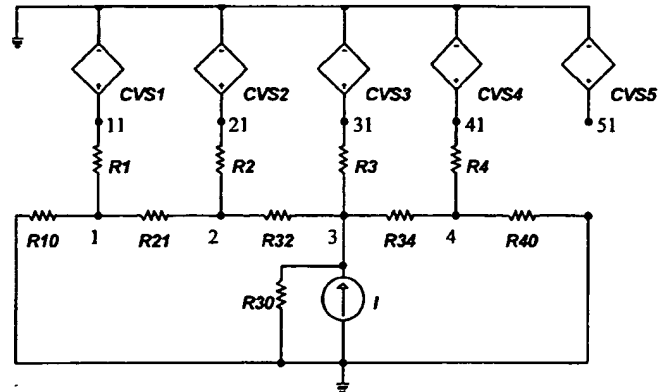

Fig. 12. Measurement and simulation of wall temperature distributions in a single-channel device at three heat power levels for a fixed DI water flow rate of 0.1 mL/min. M refers to measurements, H refers to simulation result from the homogeneous flow model, and A refers to simulation result from the annular flow model.

Fig. 13. Schematic of the thermal circuit.

$$CVS1 = I(R1) * Rw/2,$$
$$CVS2 = CVS1 + I(R1) * Rw/2 + I(R2) * Rw/2,$$
$$CVS3 = CVS2 + I(R2) * Rw/2 + I(R3) * Rw/2,$$
$$CVS4 = CVS3 + I(R3) * Rw/2 + I(R4) * Rw/2,$$
$$CVS5 = CVS4 + I(R4) * Rw/2$$

by the microchannel flow. A detailed internal flow model that considers both single and two-phase flow is developed to simulate pressure and temperature distribution with finite volume method. By applying energy balance equations and using classical heat transfer coefficient fittings, the simulation and measurement results are in reasonable agreement.

A. Heat Loss Estimation

A thermal circuit has been developed to estimate the heat loss in the test system. Heat loss here is defined as the fraction of the input power that is carried away by anything other than the fluid.

As shown in Fig. 13, the internal fluid flow (single phase) is modeled as controlled voltage sources (CVS). R_w is the equivalent resistance of convective flow with heat exchange ($1/\dot{m}c_p$, where $\dot{m}$ is the mass flow rate, and c_p is the liquid specific heat).

THERMAL RESISTANCES OF A SINGLE-CHANNEL DEVICE

Resistance	Value (K/W)
R$_w$ (1/ $\dot{m}$ c$_p$, fluid)	143.5
R1 (1/hA, reservoir)	13.8
R2 (1/hA, entrance)	0.5
R3 (1/hA, microchannel)	3.8
R4 (1/hA, exit)	0.5
R21 (l/kA, entrance-reservoir)	80
R32 (l/kA, channel-entrance)	300
R34 (l/kA, channel-exit)	300
R10 (fixture, estimated)	75
R40 (fixture, estimated)	130
R30 (device, estimated)	300

Nodes 1 through 4 are the average temperatures of inlet reservoir, entrance region, microchannel, and the exit region (shown in Figs. 1 and 2). Nodes 11 through 41 are the average temperatures of the fluid in the corresponding sections, and node 51 is the outlet fluid temperature. R1 to R4 are forced convective resistances (1/hA, where h is convective coefficient, and A is convective area); R10 and R40 represent the sum of device-system contact resistance, system conductive, free convective and radiative resistances; R30 is free convective and radiative resistance of the device; R21, R32, and R34 are conductive resistances in silicon (l/kA, where l is the length, k is thermal conductivity of silicon, and A is cross-sectional area).

Ideally, all heat power, which is modeled as the current source I, should go through R3 (forced convection in the microchannel) and cause fluid temperature rise. However, there exists heat loss from the device as well as the system in reality, which is reflected by the current in other resistors in the circuit. By simulating the current in all resistors, we can predict the heat distribution in the system.

The thermal circuit analysis suggests that the system heat loss due to conduction in silicon can be limited by adjusting the ratio of R3 to other resistors, that is, changing the geometry of the test chip. The model has been used to design the dimensions of the reservoir and channel wall thickness so as to maximize the thermal conduction resistance in these regions. As an example, Table II lists the resistance values of Device 2, a 50 -μm wide and 70 -μm deep single-channel design, at 0.1 mL/min flow rate.

The thermal resistance for conduction through the silicon between the resistor and the fluid-wall interface is approximately 0.23 K/W (single-channel) or 0.06 K/W (multichannel), while the convection resistance into the fluid is never smaller than 3.8 K/W. As a result, the thermometers provide an accurate measure of the wall temperature.

The model also suggests that increasing flow rate is an effective method to reduce heat loss. For example, at 0.5 mL/min flow rate, the system heat loss in Device 1 is as low as 5%, with 5% preheating. However, large flow rates may be detrimental because the local temporal pressure increase during phase change is severe in microchannels in this dimension. Even silicon-glass bonds that survive 500 kPa static pressure could be broken by the boiling, which has been observed in our experiments. Therefore, we chose 0.1 mL/min flow rate in above experiments. Larger flow rates will be tested in future studies.
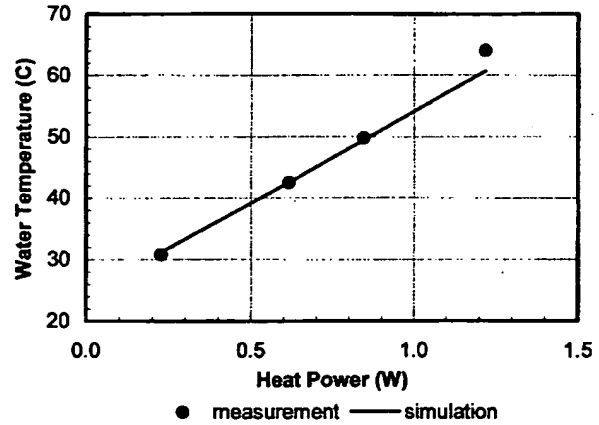

Fig. 14. Outlet water temperature measurement and simulation.

The measured and estimated exit water temperature during single-phase heat transfer experiments on Device 2, are plotted together in Fig. 14. The measurements and simulations are in good agreement, indicating that the model accounts well for the various heat transfer paths in the device. We use this model to estimate the fraction of the system heat loss to the fixture and environment as well as the fraction of the heat carried away by the fluid.

At 0.1 mL/min flow rate, the estimated system heat loss for Device 1 (40-channel design) is 39%, with 20% lost to preheating of inlet water. The system heat loss for Device 2 (single-channel design) is 26%, with 12% lost to preheating.

With the thermal circuit model, we have an accurate description of the heat transfer in the system during single-phase fluid behavior. Therefore, we can now focus on the heat transfer inside the microchannel in the two-phase case.

B. Phase Change Simulation

A 1-D microchannel flow and heat transfer simulation is developed for comparison with the experimental results [13]. The simulation numerically solves energy equations for heat conduction in the silicon wall and convection by the fluid, with boundary conditions dictated by the heat loss to the environment. The simulation uses the finite volume method and considers the temperature and pressure dependence of the liquid and vapor properties based on correlations to tabulated data.

The simulation is 1-D in the direction along the channel and uses average local temperatures for the solid wall and the fluid, T_w and T_f, respectively. The energy equations are

$$\frac{d}{dz}\left(k_w A_w \frac{dT_w}{dz}\right) - \eta h_{conv} p(T_w - T_f)$$
$$- \frac{w(T_w - T_\infty)}{R_{env}} + q''w = 0 \qquad (1)$$

$$\dot{m}\frac{di_f}{dz} - \eta h_{conv} p(T_w - T_f) = 0 \qquad (2)$$

where z is the coordinate along the channel, A_w is the channel wall cross-sectional area, p is the perimeter of the channel cross section, and w is the pitch of one channel. The fin effectiveness, η, accounts for the temperature variation normal to the heat sink within the local channel walls. k_w is the thermal conductivity of

silicon, $\dot{m}$ is the mass flow rate, and h_{conv} is the convection coefficient for heat transfer between the channel wall and the fluid. The fluid enthalpy per unit mass, i_f, for two-phase flow is expressed in terms of local fluid quality x, which is the mass fraction of the vapor phase, using

$$i_f = (1 - x)i_l + xi_v \qquad (3)$$

where subscripts l and v refer to liquid and vapor phase in two-phase flow, respectively. Equation (1) accounts for heat conduction along silicon wall in the first term, convection heat transfer rate in the second term, and the natural convection heat loss to the environment using the resistance R_{env} in the third term. Radiation heat loss is neglected due to its very small magnitude. The fluid flow equation (2) relates the change of the average enthalpy density of the fluid against the heat transfer rate into the fluid from the channel walls.

Two flow models are proposed for the two-phase regime. A homogeneous flow model assumes that the liquid and vapor have the same velocity at every position z. The other approach is annular two-phase flow model, which assumes that a thin, slow-moving liquid film surrounds a rapidly moving core of vapor. The data of Stanley et al. [14] for heat flux and friction coefficient for two-phase flow along channels of comparable dimensions lend more support to the homogeneous flow model. The pressure distribution is governed by

$$-\left(\frac{dP}{dz}\right) = \frac{fm''^2}{2\rho D} + \frac{d}{dz}\left(\frac{m''^2}{\rho}\right) \qquad (4)$$

for the homogeneous model and by

$$-\left(\frac{dP}{dz}\right) = \frac{2\tau_i}{D/2 - \delta} + \frac{m''^2}{\alpha}\frac{d}{dz}\left(\frac{x^2}{\alpha\rho_v}\right) \qquad (5)$$

for the annular model, respectively. ρ is the density of the liquid-vapor mixture, ρ_v is the density of vapor phase, f is the globally averaged friction factor, and D is the channel hydraulic diameter. The mass flux m'' is related to the mass flow rate $\dot{m}$ by $m'' = \dot{m}/A_c$, where A_c is the cross-sectional area of the flow passage. δ is the liquid film thickness, τ_i is the shear stress at liquid-vapor interface in annular flow model, and α is void fraction, which is the ratio of the vapor flow cross-sectional area to the total flow cross-sectional area. The friction factor f and the convection coefficient are taken from experimental correlations and are discussed in detail in [13].

The experimental data are compared with the simulation results in Figs. 10 and 12. Fig. 10 shows reasonably good agreement between predictions and measurement data for the pressure drop as a function of applied heat power, particularly for the homogeneous model. The decreasing of the pressure drop with increasing power for powers below 1.32 W results from the decreasing viscosity of the purely liquid phase. The calculations underpredict the pressure drop in this regime due to fluid preheating in the inlet reservoir. The pressure increase with increasing power in the two-phase regime results from the acceleration of the evaporating liquid into the vapor phase. The annular flow model yields less pressure drop than the homogeneous model since it does not include the mixing effect on pressure drop.

Fig. 12 compares predictions and experimental data for the wall temperature distribution along the channel. Relatively poor agreement exists in the middle of the channel for 0.61 W power and the entry region for 2.12 W. The deviation for 0.61 W almost certainly results from an error in the value of the environmental thermal resistance, R_{env} in (1). The deviation for 2.12 W is probably due to the effects of liquid preheating. The simulations are reasonably effective at predicting the temperature magnitude and the onset of boiling. Although they do not provide sufficient detail to choose between the annular and homogeneous models, the pressure drop data lend support to the homogeneous model. Since the pressure field evaluated by the annular flow model is lower than that of homogeneous model, its corresponding saturated-temperature field is also lower than that of homogeneous model. The qualitative agreement provides support for the convection coefficient correlation, which has not previously been applied to channels with hydraulic diameters below 500 μm.

VII. CONCLUSION

We have developed silicon test devices with nearly-constant heat flux boundary conditions to study forced boiling convection in microchannels. Rectangular channels with hydraulic diameters between 25 and 60 μm and aspect ratios between 1 and 3.5 were fabricated and tested, and we recorded the pressure and wall temperature distribution during phase change. A thermal circuit model and a detailed two-phase microchannel flow model yielded predictions in reasonable agreement with the measured pressure drop and wall temperature distribution. Both models should prove very useful for microchannel design. The experiments show that boiling occurs in plasma-etched microchannels with these dimensions without excessive superheating.

REFERENCES

[1] D. B. Tuckerman and R. F. W. Pease, "High-performance heat sinking for VLSI," *IEEE Electron Device Lett.*, vol. EDL-2, pp. 126–129, May 1981.

[2] V. K. Samalam, "Convective heat transfer in microchannels," *J. Electron. Mater.*, vol. 18, no. 5, pp. 611–618, Sept. 1989.

[3] R. W. Knight, D. J. Hall, J. S. Goodling, and R. C. Jaeger, "Heat sink optimization with application to microchannels," *IEEE Trans. Compon., Hybr., Manufact. Technol.*, vol. 15, pp. 832–842, Oct. 1992.

[4] X. F. Peng, H. Y. Hu, and B. X. Wang, "Boiling nucleation during liquid flow in microchannels," *Int. J. Heat Mass Transfer*, vol. 41, no. 1, pp. 101–106, Jan. 1998.

[5] ——, "Flow boiling through V-shaped microchannels," *Experimental Heat Transfer*, vol. 11, pp. 87–100, Mar. 1998.

[6] L. Jiang and M. Wong, "Phase change in microchannel heat sinks with integrated temperature sensors," *J. Microelectromech. Syst.*, vol. 8, pp. 358–365, Dec. 1999.

[7] Y. P. Peles, L. P. Yarin, and G. Hetsroni, "Steady and unsteady flow in a heated capillary," *Int. J. Multiphase Flow*, vol. 27, no. 4, pp. 577–598, Apr. 2001.

[8] D. B. R. Kenning and Y. Yan, "Saturated flow boiling of water in a narrow channel: Experimental investigation of local phenomena," *IChemE Trans. A, Chem. Eng. Res. Design 79 (A4)*, pp. 425–436, May 2001.

[9] R. Hopkins, A. Faghri, and D. Khrustalev, "Critical heat fluxes in flat miniature heat sinks with micro capillary grooves," *J. Heat Transfer*, vol. 121, no. 1, pp. 217–220, Feb. 1999.

[10] M. B. Bowers and I. Mudawar, "High flux boiling in low flow rate, low pressure drop mini-channel and micro-channel heat sinks," *Int. J. Heat Mass Transfer*, vol. 37, no. 2, pp. 321–332, Jan. 1994.

[11] L. Zhang, S. S. Banerjee, J. Koo, D. J. Laser, M. Asheghi, K. E. Goodson, J. G. Santiago, and T. W. Kenny, "A micro heat exchanger with integrated heaters and thermometers," in *Proc. Solid State Sensor and Actuator Workshop*, June 2000, pp. 275–280.

[12] L. Zhang, J. Koo, L. Jiang, K. E. Goodson, J. G. Santiago, and T. W. Kenny, "Study of boiling regimes and transient signal measurements in microchannels," in *Proc. Transducers'01*, vol. 2, June 2001, pp. 1514–1517.

[13] J. Koo, L. Jiang, L. Zhang, P. Zhou, S. S. Banerjee, T. W. Kenny, J. G. Santiago, and K. E. Goodson, "Modeling of two-phase microchannel heat sinks for VLSI chips," in *Proc. Int. MEMS Workshop*, Jan. 2001, pp. 422–426.

[14] R. S. Stanley, R. F. Barron, and T. A. Ameel, "Two-phase flow in microchannels," in *Proc. ASME IMECE*, vol. DSC-62, Nov. 1997, pp. 143–152.

Lian Zhang received the B.S. degree in engineering from Beijing Institute of Technology in 1994, and the M.S. degree in mechanical engineering from Tsinghua University, China, in 1997. She has been working toward the Ph.D. degree in mechanical engineering at Stanford University, Stanford, CA, since 1997 under a Stanford Graduate Fellowship. She worked on piezoresistive microflow sensors as her Master's thesis.

Her current research interests include MEMS sensor design, thermal management for high-power electronics, and individual chip cooling technology such as microchannel and microjet impingement cooling.

Jae-Mo Koo received the B.S. and M.S. degrees in mechanical engineering from Hongik University, Seoul, Korea, in 1994 and 1996, respectively. He received the M.S. degree from the University of Wisconsin, Madison, in mechanical engineering in 1999.

From 1997 to 1998, he worked for Korea Institute of Science and Technology, Seoul, Korea. Currently, he is working toward the doctoral degree at Mechanical Engineering Department, Stanford University, Stanford, CA. His research interests are focused on the microscale heat transfer, microfluidics, MEMS, advanced electronic cooling technology, and electronic/MEMS packaging.

Linan Jiang (S'99–M'00) received the B.S. and M. S. degrees in aerodynamics from Nanjing University of Aeronautics and Astronautics, China, in 1987 and 1990, respectively, and the Ph.D. degree from The Hong Kong University of Science and Technology, in 1999.

She is currently a Research Associate at Stanford University with Department of Mechanical Engineering. Her current research interests include microscale heat transfer and fluid mechanics, novel microdevices and integrated microsensors, advanced cooling technology, electronic/MEMS packaging technology, and advanced micromachining technology.

Mehdi Asheghi (M'00) received the mechanical engineering degree from Sharif University of Technology and the Ph.D. degree from Stanford University, Stanford, CA, in 1999.

In 2000, he joined Carnegie Mellon University, Pittsburgh, PA, where he is now an Assistant Professor. His research interests include the thermal design of transistors, sensors, and actuators for integrated circuits, magnetic writing devices and microelectromechanical systems (MEMS) as well as the fundamental study of heat transport in very small length and/or time scales. He has made contributions to the understanding of thermal transport in thin silicon layers by measuring the thermal conductivity of nearly pure and doped single crystalline silicon layers in the order of one micron thickness, and by refining a theory that accounts for the reduction in thermal conductivity of silicon layers due to size effect and additional impurities.

Kenneth E. Goodson (M'95–A'96) received the B.S., M.S., and Ph.D. degrees in mechanical engineering from the Massachusetts Institute of Technology (MIT), Cambridge, in 1989, 1991, and 1993, respectively.

Currently, he is an Associate Professor of Mechanical Engineering at Stanford University, Stanford, CA. Previously, he worked with the Materials Research Group at Daimler–Benz AG on the thermal design of power circuits. In 1994, he joined Stanford University, where his research group studies thermal transport phenomena in electronic micro- and nanostructures. His research has yielded 80 journal and conference papers and four book chapters.

Dr. Goodson has received the ONR Young Investigator Award and the NSF CAREER Award in 1996, Best Paper Awards at SEMI-THERM in 2001, and the Multilevel Interconnect Symposium in 1998. In 1996, he was a JSPS Visiting Professor at the Tokyo Institute of Technology. In 1999, he received the Outstanding Reviewer Award from the *ASME Journal of Heat Transfer*.

Juan G. Santiago (M'99–A'99) received the Ph.D. degree in mechanical engineering from the University of Illinois at Urbana-Champaign (UIUC).

From 1995 to 1997, he was a Senior Member of the Technical Staff at the Aerospace Corporation and from 1997 to 1998, he was a Research Scientist at UIUC's Beckman Institute. Since 1998, he has been an Assistant Professor of Mechanical Engineering at Stanford University, Stanford, CA, where he specializes in microscale fluid mechanics, microscale optical flow diagnostics, and microfluidic system design. His research includes the investigation of transport phenomena and optimization of systems involving microscale fluid pumping, electrophoretic injections and separations, sample concentration methods, and rapid micromixing processes. The applications of this research include microfabricated bioanalytical systems for drug discovery and cooling systems for microelectronics.

Thomas W. Kenny received the B.S. degree in physics from the University of Minnesota, Minneapolis, in 1983 and the M.S. and Ph.D. degrees in physics from the University of California, Berkeley, in 1987 and 1989, respectively.

He has worked at the Jet Propulsion Laboratory, where his research focused on the development of electron-tunneling-based microsensors and instruments. Since 1994, he has been on the Faculty of the Mechanical Engineering Department, Stanford University, Stanford, CA. He currently oversees graduate students in the Stanford Microstructures and Sensors Laboratory, whose research activities cover a variety of areas such as advanced tunneling sensors, piezoresistive sensors, cantilever arrays, fracture in silicon, and the mechanical properties of biomolecules, cells, insects, and small animals. This group is collaborating with researchers from the IBM Almaden and Zurich Research Centers on nuclear magnetic resonance microscopy and AFM thermomechanical data storage, and with the Bosch RTC on inertial sensors and packaging, and with Intel on fluidic cooling technologies for integrated circuits.